ELEMENTA
Science of the Anthropocene

Boisier, JP, et al. 2018. Anthropogenic drying in central-southern Chile evidenced by long-term observations and climate model simulations. *Elem Sci Anth,* 6: 74. DOI: https://doi.org/10.1525/elementa.328

RESEARCH ARTICLE

Anthropogenic drying in central-southern Chile evidenced by long-term observations and climate model simulations

Juan P. Boisier[*,†], Camila Alvarez-Garreton[*,‡], Raúl R. Cordero[§], Alessandro Damiani[§,‖], Laura Gallardo[*,†], René D. Garreaud[*,†], Fabrice Lambert[*,¶], Cinthya Ramallo[*,†], Maisa Rojas[*,†] and Roberto Rondanelli[*,†]

The socio-ecological sensitivity to water deficits makes Chile highly vulnerable to global change. New evidence of a multi-decadal drying trend and the impacts of a persistent drought that since 2010 has affected several regions of the country, reinforce the need for clear diagnoses of the hydro-climate changes in Chile. Based on the analysis of long-term records (50+ years) of precipitation and streamflow, we confirm a tendency toward a dryer condition in central-southern Chile (30–48°S). We describe the geographical and seasonal character of this trend, as well as the associated large-scale circulation patterns. When a large ensemble of climate model simulations is contrasted to observations, anthropogenic forcing appears as the leading factor of precipitation change. In addition to a drying trend driven by greenhouse gas forcing in all seasons, our results indicate that the Antarctic stratospheric ozone depletion has played a major role in the summer rainfall decline. Although average model results agree well with the drying trend's seasonal character, the observed change magnitude is two to three times larger than that simulated, indicating a potential underestimation of future projections for this region. Under present-day carbon emission rates, the drying pathway in Chile will likely prevail during the next decades, although the summer signal should weaken as a result of the gradual ozone layer recovery. The trends and scenarios shown here pose substantial stress on Chilean society and its institutions, and call for urgent action regarding adaptation measures.

Keywords: Chile; Climate change; Drying trends; Drought; Greenhouse gas and ozone depletion; Southern annular mode

Introduction

The intensification of the global hydrological cycle that follows the atmospheric warming and moistening (Held and Soden, 2000; Allen and Ingram, 2002; Trenberth et al., 2005; Donat et al., 2016) is a notable footprint of the Anthropocene with severe and pressing consequences on human society and ecosystems (e.g., Rockström et al, 2014). However, even though mean global precipitation is expected to increase in response to the anthropogenic forcing, the patterns of precipitation change are far from being uniform and extensive regions are getting dryer, notably within the subtropics (Milly et al., 2005; Held and Soden 2006; Cai et al., 2012; Collins et al., 2013; Schewe et al., 2014; He and Soden, 2017). Most of these regions have limited water resources today and are therefore threatened by future rainfall decline and drought-related hazards (IPCC, 2012; Hagemann et al., 2013; Schewe et al., 2014; Jiménez Cisneros et al., 2014; Mekonnen and Hoekstra, 2016). Subtropical Chile may be viewed as a paradigmatic case of such vulnerable regions. A particularly consistent rainfall decline pattern is simulated in the southeast Pacific sector by current climate models in response to anthropogenic forcing (Collins et al., 2013; Christensen et al., 2013; He and Soden, 2017), some cases projecting deficits of up to 40% towards the end of the century (Polade et al., 2017). This regional effect of climate change would directly affect central-southern Chile, the region that concentrates most of the country's population and economic activities.

Changes in the hydrological regime in Chile is recognized as a major risk for the country's future development (MMA, 2016). Chile's economy over relies on natural resources, being the most material-intensive among the member

* Center for Climate and Resilience Research (CR2, FONDAP 15110009), CL
† Department of Geophysics, Universidad de Chile, Santiago, CL
‡ Instituto de Conservación, Biodiversidad y Territorio, Universidad Austral de Chile, Valdivia, CL
§ Department of Physics, Universidad de Santiago de Chile, Santiago, CL
‖ Center for Environment Remote Sensing, Chiba University, Chiba, JP
¶ Department of Physical Geography, Pontificia Universidad Católica de Chile, Santiago, CL
Corresponding author: Juan P. Boisier (jboisier@dgf.uchile.cl)

states of the Organization for Economic Cooperation and Development (OECD/ECLAC, 2016). The major economic sectors – notably agriculture and mining – and an important fraction of electric power generation (about 30%) depend on the fresh water supply via precipitation, which therefore constitutes a critical factor for the country's societal functioning. Hence, potential loss of water resources via rainfall deficit and enhanced evaporation makes Chile particularly vulnerable to climate change (Vicuña et al., 2012, Demaria et al., 2013, Magrin et al., 2014; CR2, 2015; MMA, 2016; Bozkurt et al., 2018).

If global greenhouse gases (GHG) emissions continue unabated, the future climate in Chile could look like the condition observed from 2010 to the present. In this period, central-southern Chile experienced the longest and more extended drought since ca. 1900, with just one or two similar events in the last millennium (Garreaud et al., 2017). These recent years have been characterized by annual rainfall deficits ranging from 15 to 45%, a matching reduction in surface and underground water resources, detrimental impacts on vegetation and very active fire seasons (Garreaud et al., 2017; González et al., 2018). Unsurprisingly, this drought was perceived by most of the population, although its impacts in rural areas were more direct and more detrimental than in urban settings (Aldunce et al., 2017).

Notwithstanding the robustness of the drying scenario shown by climate model simulations in the southeast Pacific sector and central-southern Chile (e.g., Polade et al., 2017), the historical and future hydrological changes in this region have been sparsely evaluated within the global climate change context. Previous studies have reported drying patterns along the southwest coast of South America (e.g., Aceituno et al., 1993; Minetti et al., 2003; Haylock et al., 2006; Quintana and Aceituno, 2012) but few of them have assessed the influence of large-scale climate change on these trends (Vicuña et al., 2010; Cai et al., 2012; Purich et al., 2013). Vera and Díaz (2015) showed that the austral summer drying observed during most of the 20th century in southern Andes is consistent with that modelled in response to external climate forcing and to changes in GHGs, particularly, while no signal of change was found in simulations including only natural forcing. Contrasting an observational dataset and model simulations, Boisier et al. (2016) analyzed a recent period of particularly large rainfall decline in central Chile (1979–2014). The causes of the observed trends were found to be of both natural and anthropogenic origin, the latter accounting for about one third of the total signal. However, these results were limited to a relatively short recent period, and no distinction was made between seasons or between major anthropogenic drivers.

Here we present an integrated view of the hydrological changes in Chile. We describe first the climatology, variability, and long-term (1960–2016) trends based on an updated network of rain-gauge and river streamflow data. We then assess the large-scale context and the role of different drivers of change trough the analysis of a large ensemble of climate model simulations. Before concluding, we discuss the sensitivity of regional precipitation to global anthropogenic forcing, as well as the influence of natural variability on the historical changes.

Datasets and methods

Local precipitation and streamflow data

The observational data used in this study include local rain-gauge and streamflow records from the Weather Service (DMC) and Water Bureau (DGA) of Chile. This dataset was collected and homogenized by the Center for Climate and Resilience Research (available at: http://explorador.cr2.cl). Following the method of Boisier et al. (2016), we applied a quality-control and gap-filling procedures on the monthly precipitation and streamflow time-series from stations having records since at least 1980. After this pre-processing, records from approximately 600 rain and 400 streamflow gauging stations were available for short-term statistics (we use the 1980–2010 period to compute climatologies). The number of stations is drastically reduced to about 200 (precipitation) and 100 (streamflow) for longer-term trend calculations (1960–2016). To make a direct comparison between both variables, the river discharge measured as water volume flow were converted to mm per time unit. This conversion was performed by normalizing the streamflow data by gauge-contributing catchment area, which is provided by the CAMELS-CL dataset (Alvarez-Garreton et al., 2018).

Climate model data

To evaluate the historical and future effect of anthropogenic forcing on large-scale circulation and precipitation in the southeast Pacific region, we adopted a large dataset of fully-coupled simulations performed with Global Climate Models (GCMs; see **Tables 1** and Table S1), most of them from the Climate Model Intercomparison Project Phase 5 (CMIP5; Taylor et al., 2012). Following the diagnoses presented, we separate the model dataset on three groups.

A first group of simulations from six GCMs is used to assess the effect of changing atmospheric concentration of GHGs and of stratospheric ozone (O_3) on precipitation and sea-level pressure (SLP) during the 1960–2005 period, including three types of simulations. Two out of these three types of simulations correspond to runs forced with all external drivers (labelled *historical* in CMIP5) and runs prescribing the evolution of GHGs solely (*historicalGHG*). The third simulation type analyzed within this group is taken from CMIP5 'miscellaneous' family (*historicalMisc*), whose configuration depends on the model (Table S1). In some cases, *historicalMisc* corresponds to simulations forced by a time varying O_3 only. In other cases, the *historicalMisc* simulation includes all anthropogenic forcing excepting O_3, cases in which the O_3-driven climate change is derived as the difference between *historical* and *historicalMisc*. An additional numerical experiment, equivalent to *historicalMisc* with fixed O_3 forcing, was performed with MIROC-ESM-CHEM. More than one run per simulation type were considered for most GCMs (Table S1). Further details on the model configuration and on this group of simulations can be found in Eyring et al. (2013).

Another dataset, including outputs from 13 GCMs, is used to contrast the historical changes driven by all external forcing (natural and anthropogenic) and by natural forcing only (incl. changes in solar irradiance as well as in aerosol concentration driven by major volcanic eruptions). The two types of simulations correspond, respectively, to the CMIP5 *historical* and *historicalNat* runs (Taylor et al., 2012).

Finally, a third group of GCM data is used to evaluate the historical and future precipitation changes, as well as to quantify the uncertainties of these changes. This group consists of a large ensemble from 34 GCMs, driven by all anthropogenic forcing. Within these simulations we have included CMIP5 *historical* runs from 1960 to 2005 and projections for 2006–2099, with several runs per simulation and GCM in many cases (Table S1). The model projections assessed correspond to simulations following the Representative Concentration Pathway (RCP) 8.5, scenario that consider a large radiative forcing of 8.5 W m^{-2} toward 2100 (*rcp85*; Taylor et al., 2012). We note that our study looks at the historical precipitation changes principally. Model *rcp85* projections help us to quantify the modelled climate sensitivities to anthropogenic forcing, and the uncertainties of change under GHG emission rates similar to the current ones. To provide a range of plausible future changes in Chile is not the goal of this paper, so we do not include other scenario runs.

We recall that all GCMs involved in CMIP5 include time-varying O_3 in their historical and future-scenario simulations, accounting for the O_3 depletion in the last decades of the 20th century and the O_3 recovery expected throughout the 21st century (Eyring et al., 2013). However, the models differ in the way O_3 is considered. In some models, O_3 is calculated within a fully-interactive chemistry and the concentration of this gas varies, within other factors, in response to Ozone Depleting Substances (ODS). In the other cases, the concentration of this gas is either computed by a semi-offline scheme or simply prescribed, in most cases following the scenario of Cionni et al. (2011).

Calculation of local and regional means trends

The historical hydro-meteorological changes in Chile are assessed using 1960 as the starting year for trend calculations. This choice is constrained by the need of (1) accounting for a period long enough to minimize the role of natural, decadal-scale climate variability (e.g., Boisier et al., 2016), and (2) having a critical number of local observations to make robust regional-scale statistics (few meteorological and streamflow stations have been operating since the first half of the 20th century).

The slope of a given variable regressed on time is used to quantify temporal trends. Records of observational sites having at least 90% of data available during the target period are included in the trend analysis. The standard error estimated for the regression parameters, and the 95% confidence interval derived for slope, are used to evaluate the statistical significance of a given trend. The null hypothesis of having no trend is rejected when the slope has low probability of being zero (p-value < 0.05).

Estimates of trend components caused by the Southern Annular Mode (SAM) and the Pacific Decadal Oscillation (PDO) are also included in the analysis (hereafter we will refer to these estimates as SAM- and PDO-congruent trends). We first compute a linear regression between detrended time-series of the assessed variable and that of the SAM and the PDO indices, to get the sensitivity to the changing phases of these phenomena. The sensitivity parameters obtained are then multiplied by the temporal trend of the corresponding mode of variability to derive the trend components. We adopted the index of Mantua et al. (1997) to characterize the PDO. Four SAM indices are included to assess the historical evolution of this phenomenon and its uncertainty. Three of them are constructed as the difference between the zonal mean SLP at 40°S and 65°S, using the monthly SLP data of two long-term reanalyses (NOAA-20CR and ERA-20C) and of the HadSLP2 product (**Table 1**). The fourth index of the SAM included here is that of Marshall (2003), which is based on SLP recorded at key sites in the southern hemisphere. The same SLP-based definition of the SAM is used to get the mean state and evolution of this phenomenon in GCMs.

The trend calculation is applied in the same way in time-series of regionally-averaged variables. In this study, we focus on a comparison between the observed data and the large-scale precipitation simulated in GCMs over a domain spanning from 30°S to 48°S. This domain, including Mediterranean-climate and wet regions in central-southern Chile, is where model simulations show a predominant drying tendency in response to anthropogenic forcing (Collins et al., 2013). The model data are averaged over a box spanning these latitudes and the longitudes 80–70°W. Given the dissimilar distribution of precipitation and streamflow stations across Chile, the regional averages of local observations are first computed over smaller domains. The 30–48°S latitudinal band is divided north-south into four sub-regions of 4.5-degree of latitude. The averages over the sub-domains are then re-averaged over the larger domain, ensuring a better spatial representation.

A regional mean trend analysis based on local precipitation and streamflow data is done for two domains in central (30–39°S) and southern (39–48°S) Chile, respectively (indicated in **Figure 4**). The analysis of these smaller regions is done to distinguish changes in the Mediterranean and wet climate regimes in Chile, which roughly correspond to the central and southern boxes defined. Moreover, the streamflow records available for trend analysis are only available in central Chile. The regional means over these two smaller boxes in central and southern Chile, respectively, are computed from a pair of sub-regions of 4.5-degree of latitude.

Given that precipitation and streamflow records may include missing data, the regional averages of these variables are constructed from anomalies rather than from net values. Hence, a missing monthly value in a given station is estimated to have the mean anomaly off all other stations within the corresponding sub-region. All anomalies are computed with respect to the climatological mean of the 1980–2010 period (**Figure 1**).

To further alleviate the scale mismatch between the local and GCM data, when compared, observed and simulated rainfall trends are expressed as changes relative to the corresponding climatological means.

Table 1: Datasets used in this study. DOI: https://doi.org/10.1525/elementa.328.t1

Data type	Period	Source and reference	Description
Local observations			
Precipitation	1960–2016	DMC, DGA	Monthly rain-gauge records
Streamflow	1960–2016	DGA, CAMESL-CL (Alvarez-Garreton et al., 2018)	Monthly streamflow records, watershed boundaries
Reanalysis and products			
Sea-level pressure	1960–2016	NOAA-20CR (Compo et al., 2011), ERA-20C (Poli et al., 2013), HadSLP2 (Allan and Ansell, 2006)	The two reanalyses of the 20th century and the HadSLP2 dataset are used evaluate the historical trends in SLP trends and of the SAM index.
Global simulations			
Historical all forcing	1960–2005	CMIP5 (historical; Taylor et al., 2012)	This dataset includes full-forced historical runs from 34 GCMs. See supplementary Table S1 for details.
Historical natural only	1960–2005	CMIP5 (historicalNat; Taylor et al., 2012)	Set of simulations from 13 GCMs accounting for natural climate forcings only. See supplementary Table S1 for details.
Historical GHG only	1960–2005	CMIP5 (historicalGHG; Taylor et al., 2012)	Set of simulations from 6 GCMs accounting for changes in GHG forcing only. See supplementary Table S1 for details.
Historical O_3 only	1960–2005	CMIP5 (historicalMisc; Taylor et al., 2012), others	Set of simulations from 6 GCMs accounting for changes in stratospheric O_3 only, or for all forcings excepting O_3. See supplementary Table S1 for details.
Projections RCP8.5	2006–2099	CMIP5 (rcp8.5; Taylor et al., 2012)	Future simulations under the RCP8.5 scenario from 34 GCMs. See supplementary Table S1 for details.

Calculation of uncertainties driven by internal variability and climate sensitivity

Following a similar approach than Hawkins and Sutton (2011), we assess the modeled uncertainties for the precipitation trends presented here. We make use of the above-described large model dataset available for the CMIP5 *historical* and *rcp85* simulations, including several runs per GCM (see Table S1). The trend differences between runs performed in a single model are used to quantify uncertainty due to internal variability. The between-runs variance obtained on average from all GCMs having more than one run per simulation type is our estimate of the model-mean spread due to interval variability (S_{IA}^2). A total variance (S_{TOT}^2) is also computed from the complete ensemble of simulations. We then consider that S_{TOT}^2 results from the internal variability (S_{IA}^2) and a climate sensitivity (S_{CS}^2) components. That is:

$$S_{TOT}^2 = S_{IA}^2 + S_{CS}^2 \quad (1)$$

Hence, the residual variance (S_{TOT}^2 minus S_{IA}^2) is our estimate of the spread fraction driven by the different climate sensitivities in GCMs. Finally, we use the standard deviation as the spread metric of these two components, which are considered to be S_{IA}^2/S_{TOT} and S_{CS}^2/S_{TOT}, respectively.

Precipitation and streamflow mean state and variability in Chile

Because of its elongated shape, and the relative influence of the South Pacific and the Andes Mountains, continental Chile features several climatic zones. This heterogeneity manifests primarily as a strong north-south precipitation gradient, forming contrasting environments such as the extremely arid Atacama Desert and regions in southern Chile receiving more than 3000 mm/year on average (**Figure 1**). The orographic effect on precipitation induced by the Andes defines another noticeable character of the hydrological regime in Chile, in particular across the central and southern regions of the country, where precipitation on the mountain slopes can be two-to-three times larger than at lower elevations (Viale and Garreaud, 2015).

Precipitation in Chile takes place mostly within frontal systems embedded in the southern hemisphere westerly wind belt, which reach the continent from the southeast Pacific (e.g., Falvey and Garreaud 2007). As such, the seasonal variation in the latitudinal position and intensity of the storm track produces a marked seasonality in most regions of the country (**Figure 1c**). This seasonality is at its peak at subtropical latitudes (25–35°S), where more than 90% of the annual precipitation occurs during the austral winter semester (May to September), and weakens southwards towards a regime with a more even winter and

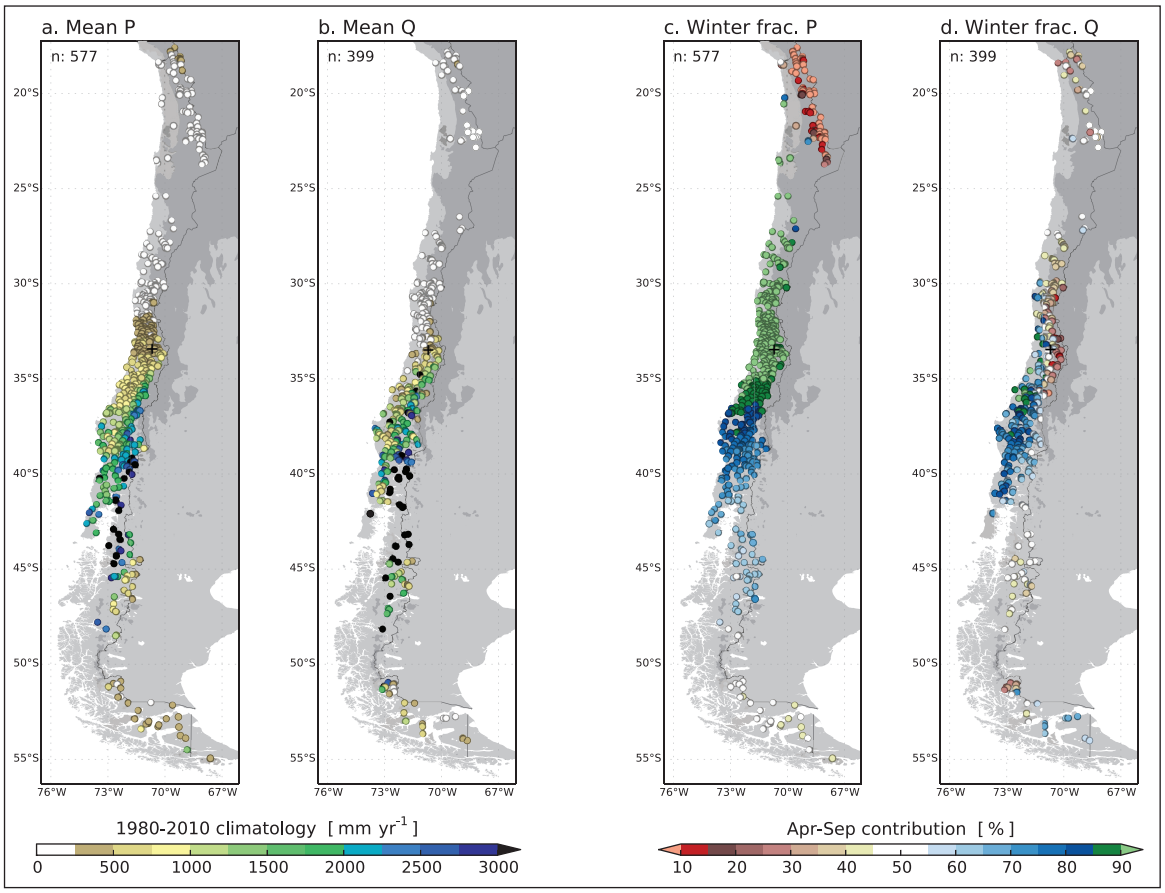

Figure 1: Precipitation and streamflow climatology in Chile. Mean annual precipitation **(a)** and normalized streamflow **(b)** in local observational sites. The contribution of austral winter semester (April–September) to annual totals for each variable are shown in panels **(c)** and **(d)**, respectively. All values are computed in stations having at least 20 years of records within the period 1980–2010. DOI: https://doi.org/10.1525/elementa.328.f1

summer precipitation in austral Chile. The precipitation regime of the Andean Plateau, at the northeastern limit of the country (Chilean Altiplano), is different from the rest of the country. The summer season peak that characterizes this regime responds to moisture advection from the interior of the continent and enhanced convection with high temperatures, which are partially controlled by the South American Monsoon (Aceituno 1998; Garreaud et al., 2003).

The amplitude and geographical patterns of annual, basin-wide mean, water flow derived from streamflow data (see Datasets and methods) match closely those of precipitation (**Figure 1b**), except in the arid regions with very low runoff coefficients. However, both variables differ in their seasonality, notably along the Andes foothills. The river discharges in these regions, with a flow maximum shifted towards spring and summer, characterize the predominantly snow-melt source of the high mountain watersheds. The spring and summer time release of water stored in the seasonal snowpack is of critical value for arid and semi-arid regions in Chile, providing most of the water supply for human consumption, irrigation and other economic activities (e.g., Vicuña et al., 2012).

Figure 2 synthesizes relevant aspects of the inter-annual precipitation variability in Chile. To dampen the biases imposed by the contrasted rainfall regimes described above, the typical amplitude of the year-to-year fluctuation is quantified through a coefficient of variation, derived as ratio of the standard deviation of the annual precipitation to the climatological mean (**Figure 2a**). This metric reveals a strong variability in central and northern Chile, where the amplitude of typical annual anomaly exceeds 50%. From a statistical point of view, the large variability affecting these arid and semi-arid regions responds to the fact that the annual accumulation integrates precipitation from only few events and during a short period of the year (**Figure 1c**), being more prone to large departures from the average. By contrast, regions with rainfall during most of the year, as in southern Chile, have a larger probability of experiencing different conditions from season to season, smoothing year-to-year fluctuations. Given these different degrees of variability, the detection (and attribution) of long-term hydrological signals represents a harder task in the northern regions than in the southern counterpart.

Beyond the seasonal aspect, there are important external controls on the precipitation regime in Chile, exerted by large-scale modes of variability. Within these modes, El Niño-Southern Oscillation (ENSO) and SAM are known as major sources of climate variability in southern South America at seasonal and inter-annual time scales, notably for precipitation in Chile (Aceituno 1988; Rutllant and Fuenzalida, 1991; Montecinos and Aceituno, 2003; Silvestri and Vera, 2003; Gillet et al., 2006; Garreaud et al., 2009). The regional rainfall sensitivity to the phase and amplitude of these large-scale phenomena, particularly

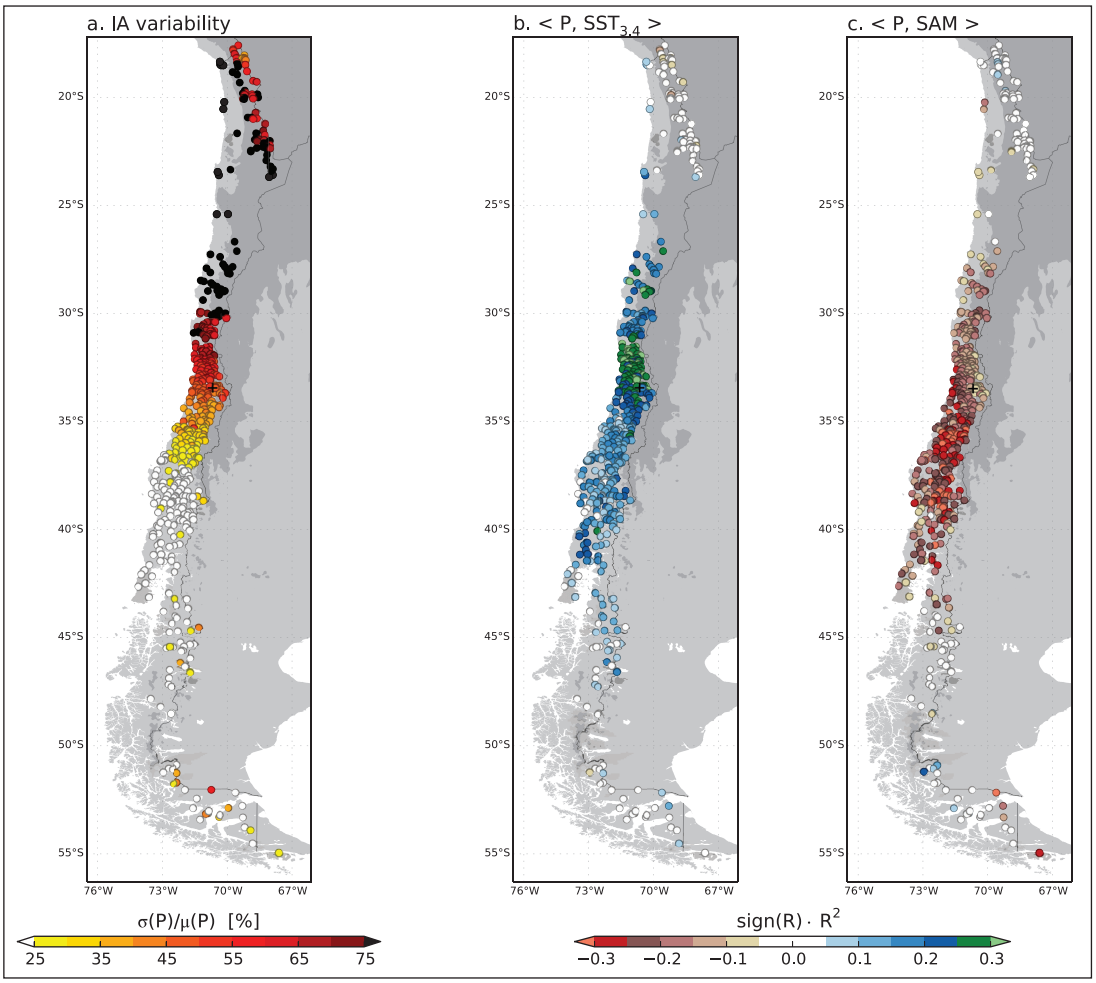

Figure 2: Interannual variability of precipitation. Standard deviation of annual precipitation normalized against the mean annual accumulation **(a)**. Covariance of annual precipitation with indices of ENSO SST 3.4 **(b)** and of the southern annual mode **(c)**. R stands for Pearson's correlation between the corresponding variables. DOI: https://doi.org/10.1525/elementa.328.f2

the one related to SAM, is a key factor to account for when evaluating long-term changes in Chile and is, therefore, re-assessed with the observational dataset used here.

In line with previous results, a clear influence of ENSO and SAM on annual precipitation is observed in the central and southern regions of Chile (**Figure 2b, c**). The warm ENSO phase is associated to wet conditions in most of the country, but is a particularly important driver for the center-northern regions (25–35°S). In turn, the positive phase of the SAM leads to negative rainfall anomalies of particularly large amplitude in central-southern regions (35–45°S). At annual time scales, these modes explain about 30% of the rainfall variance in some regions, but more geographically defined and stronger correlation patterns are found when considering seasonal averages (not shown). We note that the indices used here for ENSO and SAM (Datasets and methods) are not independent ($R^2 \sim 15\%$), so the fractions of precipitation variance explained by these modes of variability are not completely additive. Moreover, the influence of both ENSO and SAM depend on the definition or index considered (notably in the case of SAM; see e.g. Ho et al., 2012).

Given the relatively small size of watersheds in Chile, the streamflow anomalies in a given hydrological year (considered typically from April to March) follow tightly the precipitation anomalies of the corresponding calendar year. Given this strong relationship, the analysis done to characterize precipitation variability (**Figure 2**) leads to very similar results when applied to streamflow data (not shown).

Observed trends in precipitation and streamflow (1960–2016)

Annual mean trends

To introduce the trend analysis, in **Figure 3** we compare time series of annual precipitation from three rain-gauge stations in central-southern Chile, usually taken as references because of their reliable, complete and century-long records. Three time-series of watershed-normalized annual streamflow are also shown in **Figure 3**. In this case, the streamflow measuring sites were selected with the criteria of having long records (50+ years), being located at similar latitudes than the three rain-gauge stations assessed, and including Andean sectors within their contributing catchment areas. The differences in the mean precipitation and in the year-to-year variability, from *Quinta Normal* in Santiago (33.4°S, ~300 ± 150 mm yr^{-1}) to *Carriel Sur* in Concepción (36.8°S, ~1000 ± 200 mm/yr) to *El Tepual* near Puerto Montt (41.4°S, ~1700 ± 300 mm/yr), illustrates the latitudinal gradient described previously. Further, the contrast between the rain-gauge mean precipitation and the normalized

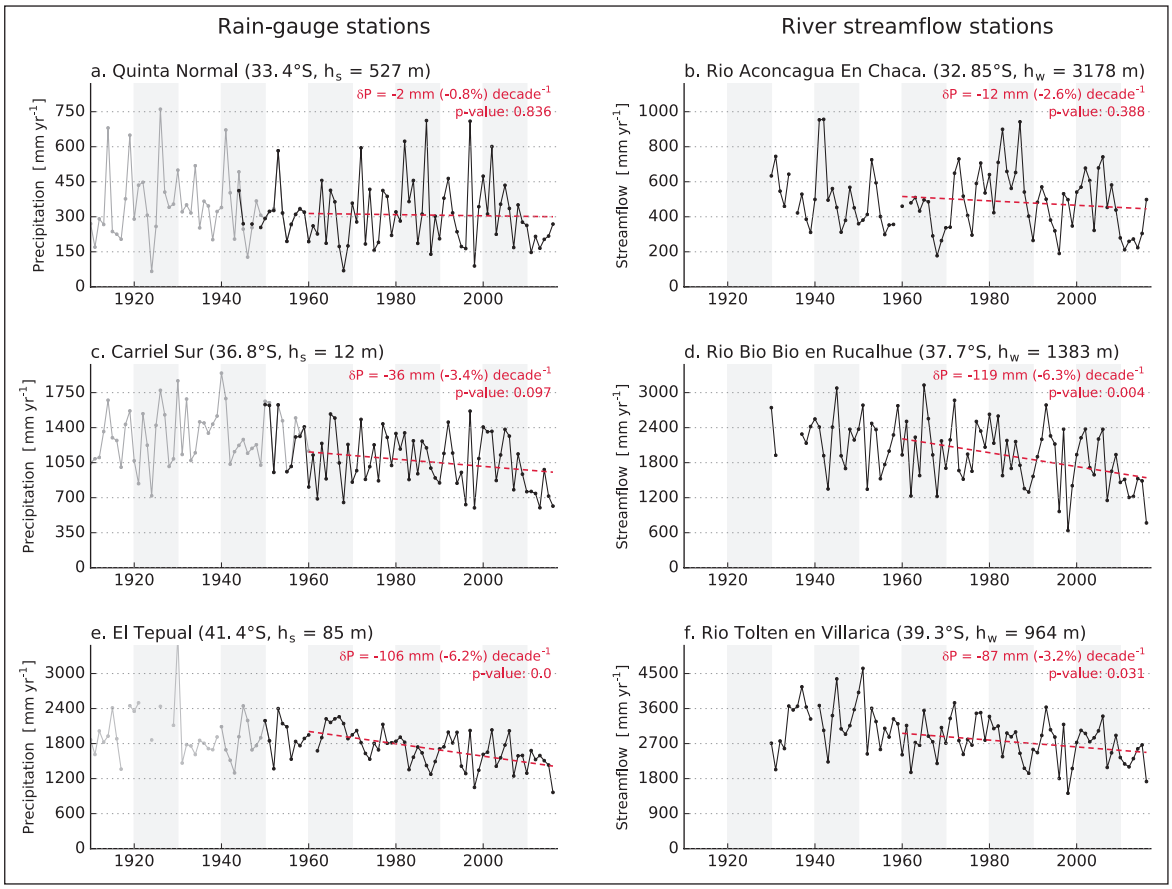

Figure 3: Precipitation and streamflow in selected locations of center-southern Chile. Time-series of annual precipitation measured at stations *Quinta Normal* **(a)**, *Carriel Sur* **(c)** and *El Tepual* **(e)**. Normalized annual streamflow at *Rio Aconcagua En Chacabuquito* **(b)**, *Rio Bio Bio en Rucalhue* **(d)** and *Rio Tolten en Villarica* **(f)**. Dashed lines shown the corresponding linear regression model for the 1960–2016 period. For each case, the temporal trend is indicated along with a two-sided p-value, indicating the probability of having a null slope. DOI: https://doi.org/10.1525/elementa.328.f3

streamflow at similar latitudes evidences the increasing rainfall with height (the mean elevation of the corresponding watershed is indicated in **Figure 3**). Given rainfall-runoff mechanisms, a noticeable positive correlation is observed between precipitation and streamflow time series. This co-variability also reveals the control of large-scale phenomena on both variables in the central-southern Chile (note, e.g., the positive and negative anomalies reached during the El Niño – La Niña transition in 1997–1998).

A predominantly negative tendency within the available periods can be noticed in the precipitation and streamflow records shown in **Figure 3**. Qualitatively, the long-term rainfall decline at *El Tepual* is large in amplitude compared to the relatively weak inter-annual rainfall variability in this location. In contrast, at *Quinta Normal* there is no clear long-term signal emerging from a background of large rainfall variability. For a quantitative comparison, the linear trends computed between 1960 and 2016 are indicated in **Figure 3**. Consistently, no long-term changes were found for the rainfall data at *Quinta Normal* nor for the streamflow at *Rio Aconcagua en Chacabuquito*. All other cases show negative trends, of particularly large amplitudes in the rainfall records at *El Tepual* and in streamflow at *Rio Bio Bio en Rucalhue* (>5% per decade).

To have a robust diagnosis of hydrological changes at a regional scale, the linear trends were computed in all rain-gauge and streamflow records satisfying the minimum data requirement within the period assessed (Datasets and methods). The mean annual precipitation and streamflow trends obtained for 1960–2016, although with some important between-sites discrepancies in the amplitude and –in few cases– in the sign of change, confirm a dominating drying pattern in most central-southern Chile (**Figure 4**). Consistent with the weak signal-to-noise value seen in Santiago (**Figure 3a**), the rain-gauge records in central Chile lead mostly to negatives but non-statistically significant rainfall trends (–1.7% per decade on average; **Figure 4a**). An interesting result to highlight is that the streamflow data within the same region indicate a decline larger in amplitude (–3.8% per decade) than the one derived for precipitation (**Figure 4b**). Since runoff is a fraction of precipitation, an amplification in streamflow trends –seen in relative term– would be expected if there were no changes in other components of the water budget. The dependency of streamflow on other processes, including evapotranspiration, snow accumulation, vegetation changes and land use may further explain distinct hydrological responses to precipitation changes. Following this stronger signal, the streamflow data also show a larger fraction of cases with trends statistically different from zero. Yet, there is also a large spread within the streamflow trends derived in this region (a standard

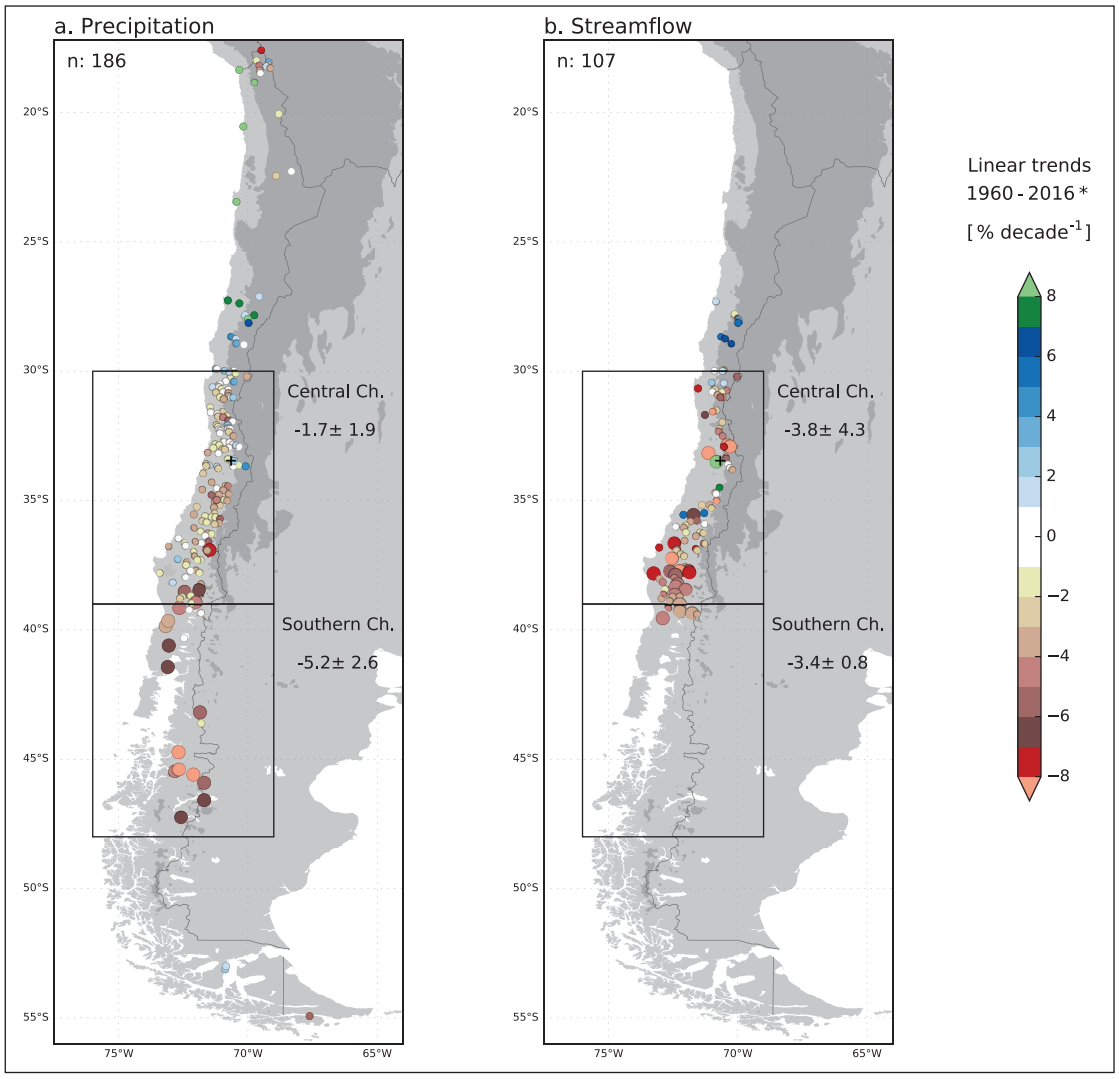

Figure 4: Changes in annual precipitation and streamflow. Linear trends of annual precipitation **(a)** and streamflow **(b)** based on local observations from 1960 to 2016. Large markers indicate locations where the corresponding trends are significantly different from zero, with a confidence interval of 95%. Boxes indicate the two domains used for regional averages, in central (30–39°S) and southern (38–48°S) Chile, respectively. *Trends are computed in stations having valid data in at least 90% of the period assessed. DOI: https://doi.org/10.1525/elementa.328.f4

deviation of 4.3 mm per decade), including a number of sites with positive values.

In southern Chile, the few rain-gauge stations with long-term records indicate a larger and more robust regional drying signal (**Figure 4a**). Almost all stations show negative trends of amplitudes exceeding 5% per decade. Most of these trends are also significantly different from zero. Unfortunately, no streamflow gauging stations with enough data are available south of 40°S for an assessment of long-term river discharge changes in southern Chile.

In addition to the drying pattern observed in central-southern Chile, our results indicate positive rainfall trends north of 30°S and in Punta Arenas (52°S) in austral Chile (**Figure 4a**). In the first case, although the hypothesis tests do not indicate any robust signal of change, the positive rainfall trends agree in sign with the streamflow trends observed at similar latitudes (**Figure 4b**). As noted above, the large variability in the semi-arid northern Chile does not allow a proper assessment of change with the methods adopted here. Given the low rainfall frequency in this region, the episodes of precipitation may be considered as extreme events. Therefore, the changes in this regime must be approached with a suitable technique and dataset (daily means at least). In Austral Chile, it is the lack of long-term meteorological data that hinders a clear diagnostic of change at the scale of the region.

Seasonal mean trends

We now look at the linear precipitation and streamflow trends separated by season and region. The focus is on two regions located in central and southern Chile, respectively (**Figure 4**; see also Datasets and methods). The seasonal mean precipitation and trends are shown both in absolute and relative terms for the two regions assessed in **Figure 5**. Given the strong rainfall seasonality in central Chile, the drying trend seen at annual scales in this region responds principally to changes during the rainy season (JJA), which averages –9.5 mm (–2%) per decade. Yet, the changes seen in relative terms indicate a stronger change in spring (SON) and summer (DJF). We note here that given the very dry summer condition in central Chile, any change compared to the climatology should be interpreted carefully.

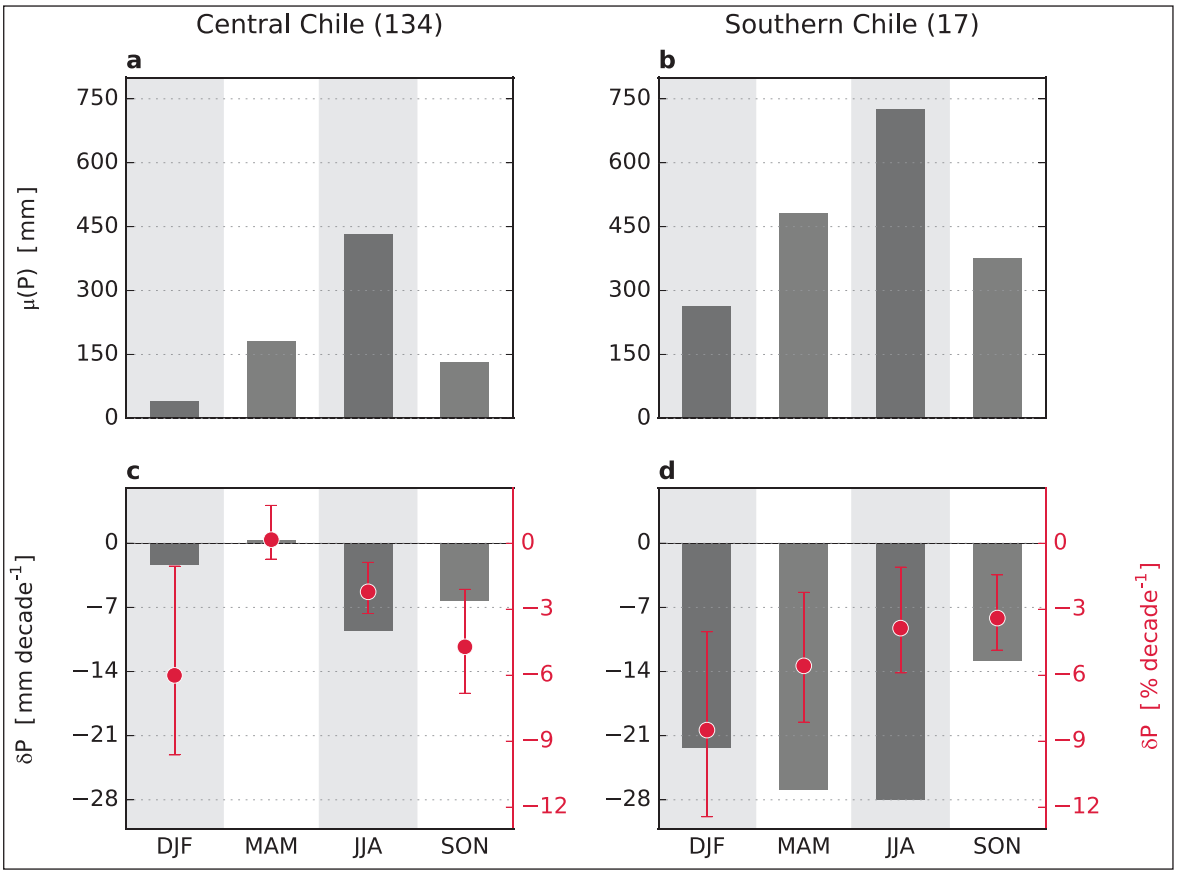

Figure 5: Regional and seasonal mean precipitation trends. Climatological mean precipitation **(a, b)** and linear trends for the period 1960–2016 **(c, d)**, derived from rain-gauge records located in central (30–39°S, a, c) and southern (39–48°S, b, d) Chile. Grey bars and red dots indicate absolute and relative trend values. Error bars indicate the trend interquartile range obtained within the stations of the corresponding region. DOI: https://doi.org/10.1525/elementa.328.f5

In southern Chile, the negative rainfall tendency represents a robust signature in all seasons (**Figure 5d**). Seen in relative terms, the trends expose a clear seasonality of change in this region, with a summer decline (~8% per decade) two times stronger than in winter (~4% per decade). As we discuss in the section that follows, these seasonal differences very likely reveal the additive influence of GHG and stratospheric O_3 forcings in this region.

Regional and seasonal mean trends in river discharge are also computed using the long-term records available in central Chile (**Figure 6**). To inquire into potential differences between rain and snowmelt-dominated regimes, the streamflow stations used for regional averages were split between those located below and above 500 m a.s.l. Even though the streamflow observed at low elevation accounts for the mountain hydrology, precipitation contribution becomes predominant and the mean streamflow seasonality follows closely the precipitation regime, with a clear maximum in JJA (**Figure 6a**). The 1960–2016 trends, in this case, are fairly consistent with those obtained for precipitation in central and southern Chile (**Figure 5c**), showing a change towards a dryer condition, of particularly large amplitude in DJF (~–8% decade) and SON (~–5.5% decade).

The hydrological seasonal pattern of change is even more pronounced when looking at the streamflow data from stations located above 500 m a.s.l (**Figure 6d**). In this case, a strong drying trend in summer and spring contrasts with the weak to even positive changes observed in winter. This particular behavior may reveal the relative influence of the Andes warming on snow accumulation and melt, leading to a shift in the runoff maximum toward earlier dates in the year (Bozkurt et al., 2018).

Large-scale drivers of change, anthropogenic forcing and future scenario

PDO and SAM-induced precipitation trends in Chile

As shown in **Figure 2**, both ENSO and SAM have a large influence on precipitation in Chile. One can maintain two differing perspectives on this influence. On one hand, given that ENSO and SAM provide an important source of variability, they add noise to local climate series, making trend detection much harder. On the other hand, if well-known, a large-scale mode of variability such as ENSO and SAM can be quantified, reducing the uncertainties in the trend attribution. For instance, Boisier et al. (2016) have shown that low-frequency ENSO-like variability in the Pacific Basin, characterized through the PDO, explains about 50% of the rainfall decline observed in central Chile in the period 1979–2014. The remaining fraction of this trend was unlikely driven by other natural phenomena, but was consistent with the simulated response to the historical anthropogenic forcing. Following a similar methodology, we explore the causes of the long-term (1960–2016) precipitation trends in Chile.

We first look at the changes in precipitation that are estimated to be forced by both the PDO and the SAM (see Datasets and methods). It is important to recall here

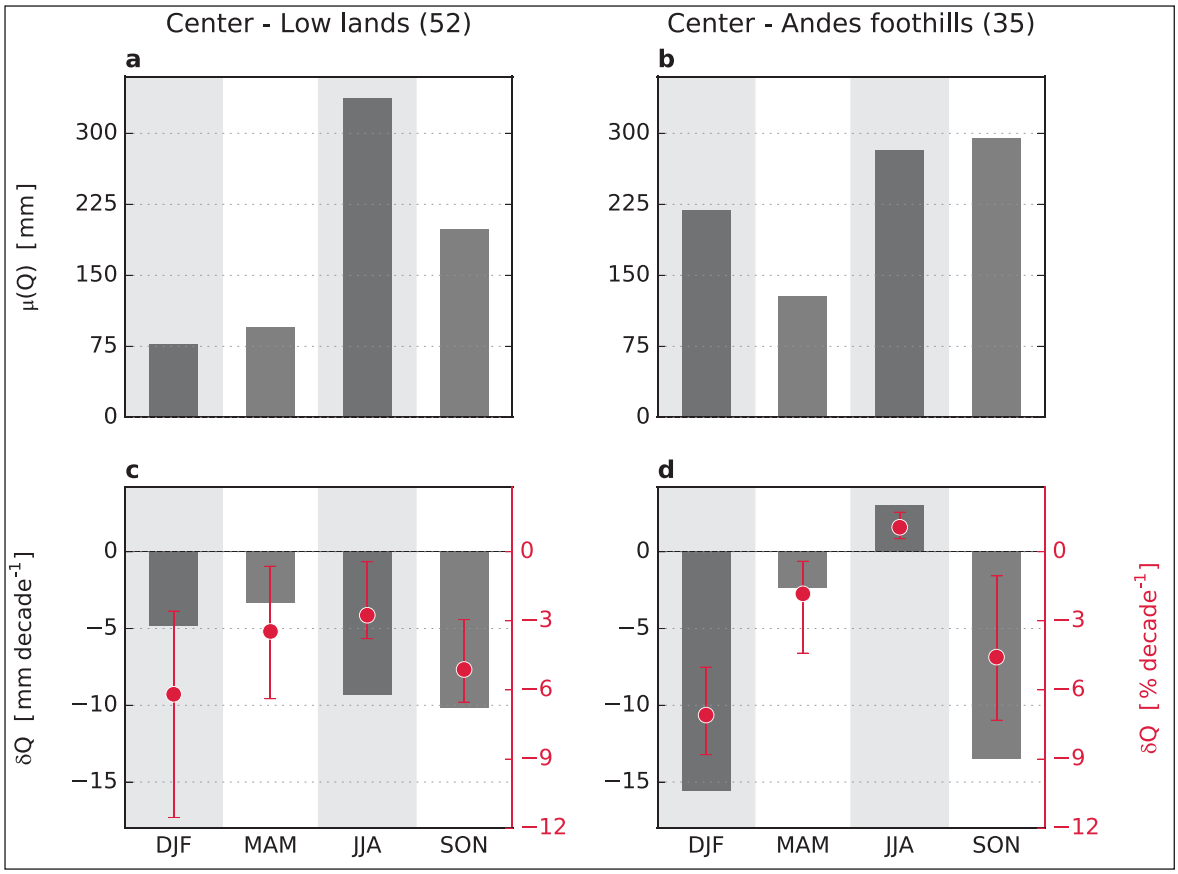

Figure 6: Regional and seasonal mean streamflow trends. Climatological mean streamflow **(a, b)** and trends for the period 1960–2016 **(c, d)**, derived from gauge records located in central Chile (30–39°S). Regional statistics are based on stations located below (a, c) and above (b, d) 500 m a.s.l. Grey bars and red dots indicate absolute and relative trend values. Error bars indicate the trend interquartile range obtained within the stations of the corresponding region. DOI: https://doi.org/10.1525/elementa.328.f6

that the evolution of these two phenomena during the period assessed is of different nature. The anthropogenic forcing likely modifies the frequency and amplitude of cold and warm events of ENSO or ENSO-like cycles such as the PDO (Cai et al., 2014), but there is no clear evidence showing a pattern of change favoring a particular phase of these phenomena. As such, we consider the trends in the PDO index as natural, transitory changes of its phase. By contrast, beyond the inherent intra-seasonal variability of the SAM, all indices used to quantify this phenomenon evidence a drift towards it positive phase during the last decades. This trend has been shown to be driven by the major global anthropogenic forcings, in particular the stratospheric ozone depletion (Cai et al., 2003; Shindell and Schmidt, 2004; Arblaster and Meehl, 2006; Karpechko et al., 2008; Fogt et al., 2009; Polvani et al., 2011; Thompson et al., 2011; Gillett et al., 2013). Therefore, we interpret the SAM-congruent rainfall trends as mostly an anthropogenic signature.

The PDO and SAM-congruent precipitation trends from 1960 to 2016 are shown for central-southern Chile in **Figure 7**. In annual time scales, the PDO does not force any significant change in this part of the country because the PDO itself does not exhibit a clear trend between 1960 and 2016 (period that includes both positive and negative PDO phases). This result contrasts with the strong drying in Chile led by the same phenomenon in the period 1979–2014 (Boisier et al., 2016). On the contrary, the trends in annual precipitation that are estimated to be driven by the SAM between 1960 and 2016 show a clear drying signature in most regions of central-southern Chile (**Figure 7b**), of similar or even larger amplitude than the actual observed trends (**Figure 4**).

The seasonal disaggregation of trends is also shown in **Figure 7**, averaged over central and southern Chile. In both regions, the SAM evolution seems to play a major role conducting negative rainfall trends, notably in DJF and MAM. This seasonal character agrees well with the rainfall trends that are actually observed in southern Chile, which are of particularly large amplitude in these seasons (**Figure 7d**). A less clear relationship is seen in central Chile, particularly in MAM, where no robust precipitation trends are derived from rain-gauge records (**Figure 7c**). As the linear analysis suggests, the weak trend in this region and season may be partially explained by a counteracting effect of the PDO and the SAM. During summer (DJF), both the SAM and the PDO appear to act in the same direction leading to a large negative rainfall trend, a feature that matches the actual trends observed in both regions. We recall the very dry summer mean condition in central Chile, so the relative trend in this season and region must be interpreted carefully.

Greenhouse gases and stratospheric ozone forcings

The SAM-driven drying in central-southern Chile (**Figure 7**) suggests that the precipitation regime in this region is being affected by global anthropogenic

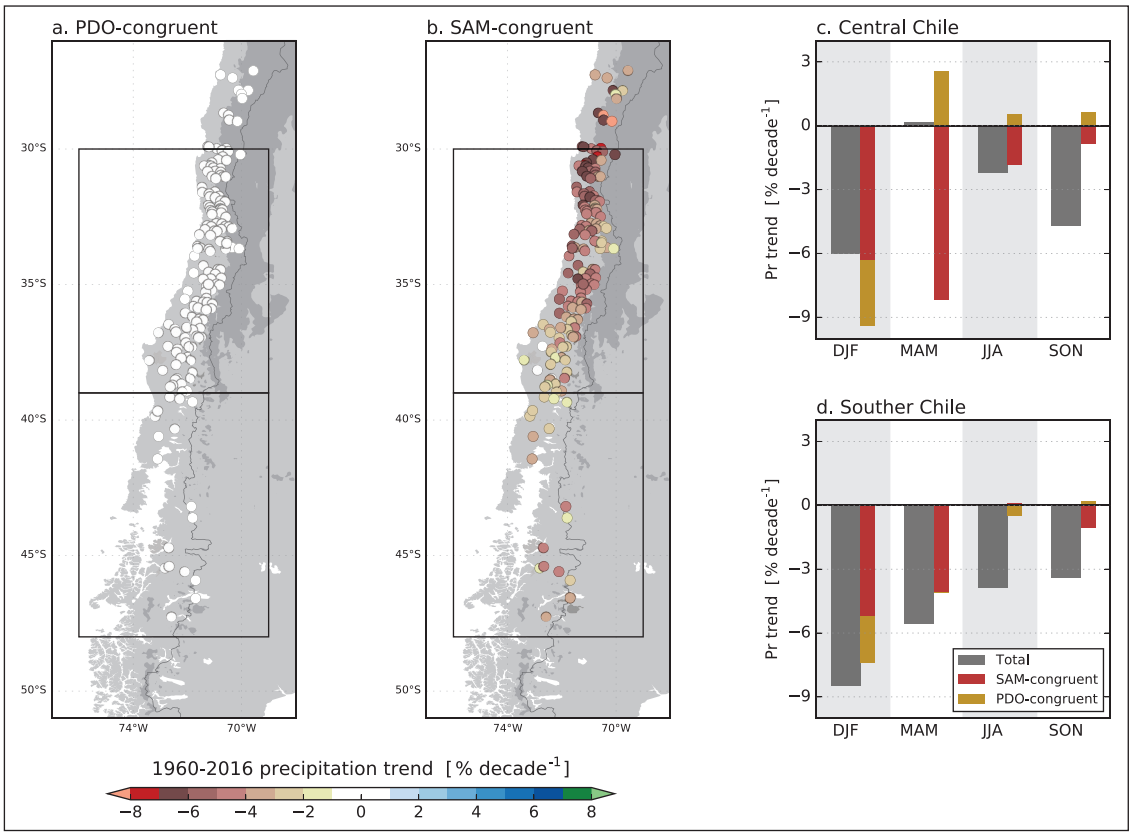

Figure 7: Precipitation trends driven by the PDO and the SAM. Annual precipitation trends (1960–2016) in central-southern Chile congruent with the PDO **(a)** and the SAM **(b)**. Total (grey), SAM-congruent (red) and PDO-congruent (orange) seasonal mean trends in central (30–39°S, **c**) and southern (39–48°S, **d**) Chile. DOI: https://doi.org/10.1525/elementa.328.f7

forcing. To further support (or call into question) this inference based solely on local observations and reanalysis data, we looked into a large ensemble of climate model simulations.

In a first stage, we analyzed a set of simulations done with six GCMs, designed to quantify the impact of the GHG and O_3 forcing separately, and a third group of simulations from the same models accounting for all the historical climate forcings (Datasets and methods). The multi-model mean trends in annual precipitation and in SLP obtained from these experiments are shown in **Figure 8**. In agreement to previous findings (e.g., Arblaster and Meehl., 2006), the ensemble of simulations gathered here shows a clear pattern of change in the southern hemisphere SLP between 1960 and 2005 (the historical period common to these runs). This pattern, like the positive SAM phase, is simulated in response to both the GHG and O_3 forcings, with trends amplitudes of the same order (about 0.3 hPa per decade, **Figure 8b, c**). The additive effect of both drivers is fairly consistent with what the full-forced simulations show on average (**Figure 8a**), notwithstanding these simulations also account for other anthropogenic (changes in the aerosols concentration and in land use) and natural climate drivers.

The SLP trends driven by GHG and O_3 represent a surface manifestation of an extratropical circulation response present in most of the troposphere and lower stratosphere (e.g., Karpechko et al., 2008; Son et al., 2010; Polvani et al., 2011). This response entails a poleward shift of the band of maximum meridional pressure gradient, westerly flow and baroclinicity. Accordingly, precipitation tends to decrease in the subtropics and mid-latitudes, and to increase south of 50°S, as shown by the simulations assessed here (**Figure 8**). The southeast Pacific and the southwest bound of South America, notably, are particularly affected by the drying tendency. Additionally, the decreased westerly flow at ~40°S impacts directly central-southern Chile by reducing the orographic rainfall component (Garreaud et al., 2013).

To synthetize the GHG and O_3-driven effects on the large-scale circulation and on the rainfall regime in Chile, the simulated changes in the SLP-based SAM index and in precipitation averaged over the central-southern Chile domain (hereafter P_{CL}, box in **Figure 8**), are shown in **Figure 9**. In the simulated period, the SAM index increases in all seasons when all climate forcings are accounted for, but shows a seasonal pattern of change characterized by a stronger signal in the austral summer (**Figure 9a**). This seasonal pattern is clearly led by the O_3 forcing, as has been shown in previous studies (e.g., Gillett et al., 2013). The GHG forcing increases the SAM polarity in the same order of magnitude than O_3, but with a weaker seasonality. It is important to highlight that both the GHG and O_3-induced changes in the SAM vary substantially from model to model (see error bars in **Figure 9**).

On average across the model simulations, the P_{CL} response to all anthropogenic forcing indicates a year-long drying pathway, but of stronger amplitude in summer (~4% per decade, **Figure 9d**). The negative trend

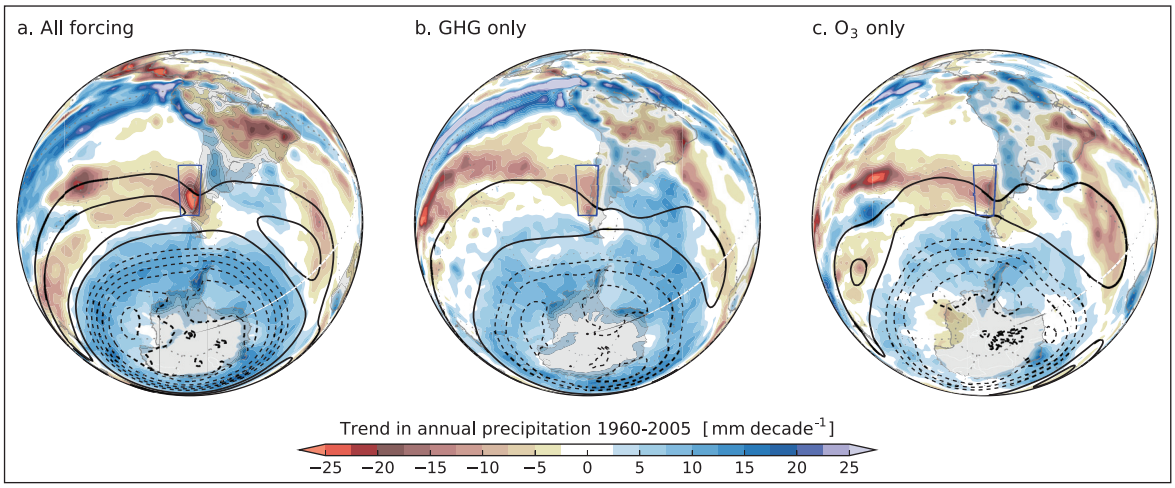

Figure 8: Simulated sea-level pressure and precipitation trends. Multi-model mean trends (1960–2005) in annual sea-level pressure (contour lines; solid and dashed contours indicate positive and negatives trends, drawn every 0.1 hPa decade^{-1}) and precipitation (color shading). Results are from the ensemble of simulations from six GCMs including all historical forcings **(a)** the greenhouse gases (GHG) forcing only **(b)** and the stratospheric ozone (O_3) forcing only. DOI: https://doi.org/10.1525/elementa.328.f8

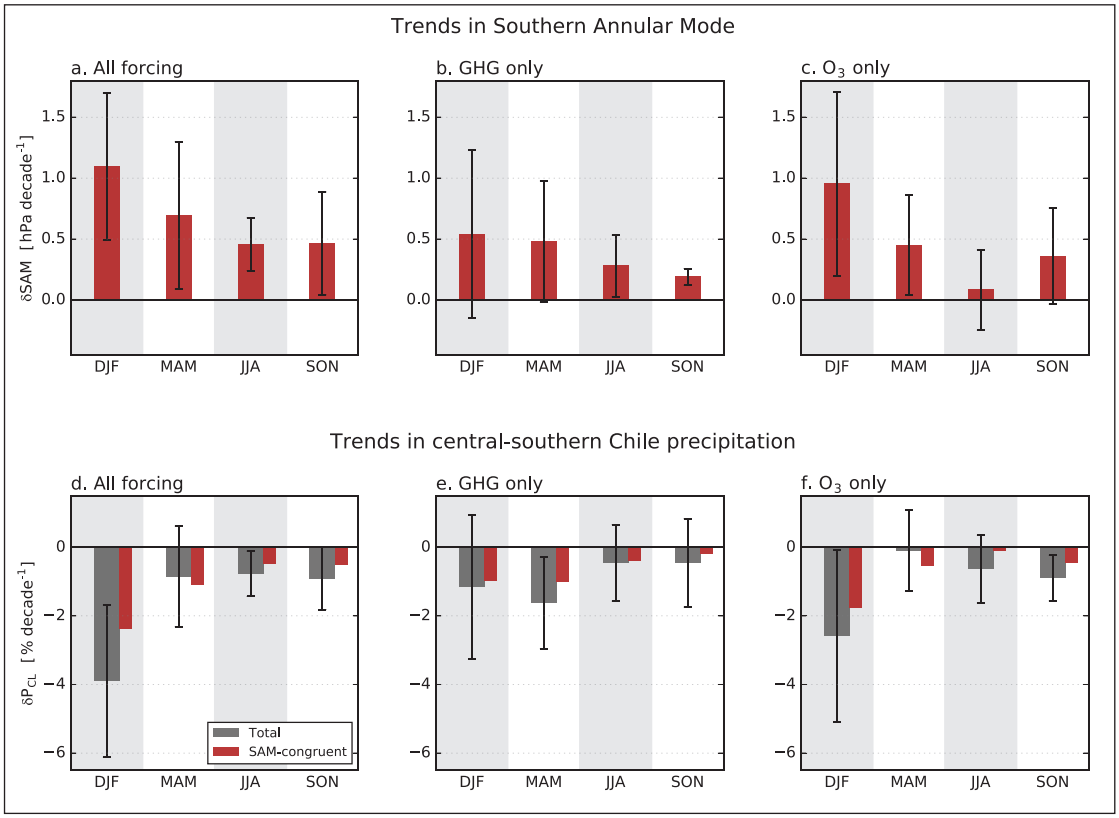

Figure 9: Simulated trends in the Southern Annular Mode (SAM) and in central-southern Chile (30–48°S) precipitation (P_{CL}). Seasonal mean trends in the SAM **(a–c)** and in P_{CL} **(d–f)** simulated by six GCMs between 1960 and 2005. Error bars indicate the multi-model mean trend and spread (standard deviation). Results are from simulations including all historical forcings (a, d), from simulations forced by GHG only (b, e) and from simulations forced by O_3 only (c, f). Red bars in bottom panels indicate the SAM-congruent changes in P_{CL}. DOI: https://doi.org/10.1525/elementa.328.f9

in P_{CL} matches fairly well the additive effects of GHG (**Figure 9e**) and O_3 (**Figure 9f**) drivers. Such as in the case of the SAM, the seasonality of change in P_{CL} is dominated by the O_3 component, which leads to a clear drying in summer and relatively weak changes through the rest of the year. Following the same procedure than for the observational data, the influence of the SAM on the P_{CL} changes is estimated in models by using the inter-annual covariability of both variables (Datasets and methods). The resulted SAM-congruent trends suggest that a major

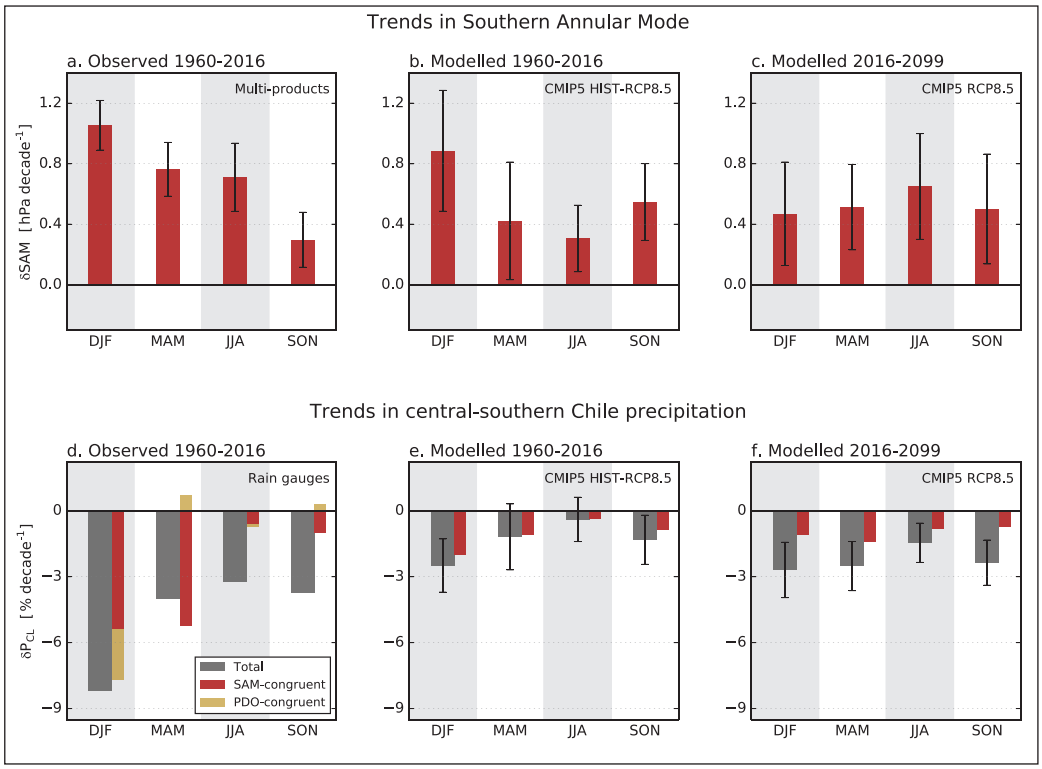

Figure 10: Observed and simulated trends in the Southern Annular Mode (SAM) and in central-southern Chile (30–48°S) precipitation (P_{CL}). Observations-based **(a, d)** and simulated **(b, e)** seasonal mean trends in the SAM (top) and in P_{CL} (bottom) between 1960 and 2016. Panels **(c)** and **(f)** show the SAM and P_{CL} trend simulated for the period 2016–2099. Model results are based on full-forced historical and RCP8.5 simulations from 33 CMIP5 GCMs (error bars indicate multi-model mean and standard deviation). Red bars in bottom panels indicate the SAM-congruent changes in P_{CL}. Orange bars in panel (d) indicate the PDO-congruent trend based on observations. DOI: https://doi.org/10.1525/elementa.328.f10

component of the simulated drying in central-southern Chile is effectively directed by the positive SAM phase-like SH circulation changes (red bars in **Figure 9d–f**).

The major control of the SAM on the modelled P_{CL} trends, and the consistent P_{CL} changes shown by full-forced simulations and the GHG-and O_3-forced simulations, point out to the anthropogenic forcing as the leading factor behind the modelled southeast Pacific drying. Previous studies have also highlighted the influence of anthropogenic forcing on long-term negative rainfall trends in this region, while no significant effect of natural forcings have been detected (e.g., Vera et al., 2015). Yet, in order to overcome doubts regarding the relative influence of external forcing on precipitation in the region and period assessed, we look also at the group of simulations prescribing natural climate drivers only (Datasets and Methods). In this case, we account for data from 13 GCMs from which we can compare the historical trends driven by all external forcings and by natural ones only (Table S1). This larger group of simulations roughly replicates the precipitation trend patterns shown in **Figures 8** and **9** when all external forcing is accounted for (see Figure S1 in supplementary material). By contrast, natural-only runs do not exhibit any robust response in the region of interest. Neither is simulated a seasonal effect of external natural forcing in the rainfall regime in Chile, therefore reaffirming that the modelled changes are mainly driven by the anthropogenic climate drivers described above.

Observed versus simulated precipitation trends, and future scenario in Chile

As the group of simulations analyzed here show, the positive SAM-like circulation trend is a robust response to both the GHG and O_3 forcings in models, and this response would have contributed to a drying tendency in the southeast Pacific region, particularly in central-southern Chile. This simulated drying occurs in all seasons, but has a maximum in summer due to the seasonal effect of O_3 depletion. Qualitatively, this modelled signature of climate change matches fairly well the precipitation and streamflow trends observed in central-southern Chile since 1960.

A direct comparison of the observations-based regional mean trends with those simulated is presented in **Figure 10**. For this comparison, the observation-based rainfall trends are averaged over the whole central-southern Chile domain (Datasets and Methods), and we use the full-forced simulations carried out within CMIP5, including runs from 34 GCMs (Table 1 and S1). The rainfall trends averaged over the central-southern Chile domain summarize the results described previously for each region separately. Such as the results based on the attribution experiments (synthesized in **Figure 9**), the focus is on the SAM and P_{CL} trends separated by season. The time frame used as reference for observations (1960–2016) is contrasted to the same period in GCM simulations, which includes historical runs until 2005 and the RCP-8.5 scenario runs for 2006–2016. To look

at the historical changes in a long-term perspective, **Figure 10** also shows the trends projected to end of the 21st century by the same group of models and under the same emission scenario.

Like the results described previously, both the observed and simulated P_{CL} indicate a major influence of the positive SAM-like circulation changes on the drying trends in Chile. The increasing polarity of the SAM shown by CMIP5 models (**Figure 10b**) matches closely the change in the SAM index obtained from the subset of models used to disentangle the contribution of GHG and O_3 (**Figure 9a**). The SAM index derived from four products based on observations (see Datasets and methods) indicates a broadly consistent behavior with that modelled, characterized by a strengthening of this phenomenon in all seasons, but of clear larger amplitude in austral summer (**Figure 10a**). In other seasons, there is less clear agreement between SAM trends derived from products and models, notably in SON. This partial mismatch may be due to a significant contribution of natural cycles to the actual trends, to different responses to external climate forcing, or to systematic biases in SLP reconstructions (Fogt et al., 2009).

The sign and seasonality of the observed P_{CL} change show a remarkable agreement with those obtained from CMIP5 ensemble (cf. **Figure 10d** and **10e**). Such as the model results, the observations-based P_{CL} indicates a negative trend in all seasons, but with an intensity markedly larger in summer than in winter. However, despite this correspondence, there is a large difference in the trends' magnitude. The P_{CL} trends based on observations are dramatically stronger than those obtained on average from the CMIP5 GCMs. This disagreement, which may have large implications on defining suitable adaptation strategies for the future changes of precipitation in Chile, is discussed further in the section that follows.

Due to the limitations for ODS emissions accorded at the Montreal Protocol, the Antarctic total ozone column has stabilized in the last decade (Solomon et al., 2016), and is expected to recover towards the end of the century (Cionni et al., 2011). This pathway, accounted for within the CMIP5 RCP scenarios (Eyring et al., 2013), manifests clearly in the modelled SAM projections, lessening or reversing the summer signal of the recent decades (Barnes et al., 2014). Accordingly, the climate projections assessed here show a consistent pathway of change in the SAM and in precipitation in central-southern Chile. On average across the GCMs, the SAM polarity continues to strengthen through the 21st century in response to the strong GHG change scenario included in RCP8.5 (**Figure 10c**). Yet, compared to the historical period, the future increase in the SAM is dampened in austral summer due to the O_3 recovery, leading to a less pronounced and, in some cases, even reversed seasonal pattern of change. The projected increase in the SAM polarity in models modulates the seasonal pattern of change in central-southern Chile precipitation, which, in contrast to the historical period with marked seasonal differences, is simulated to decrease in the future at similar rates in all seasons (**Figure 10f**).

Discussion

How can the large bias between the observed and modelled drying trend in central-southern Chile be interpreted? A first issue to consider is the scale mismatch and representativeness of spatial averages based on local observations. It should be noted that the strong drying signal shown in **Figure 10** depends substantially on the rainfall records in southern Chile (south of 40°S), a region with limited observations and important uncertainties (**Figure 4**). Another, particularly worrying reason to explain the modelled vs. observed difference would be a systematic underestimation of the southeast Pacific rainfall response to anthropogenic forcing in current GCMs. A third plausible option is that the actual negative rainfall trend has an important source of natural variability in addition to anthropogenic factor (e.g., Muñoz et al., 2016).

To further explore this last point, we look closer at the uncertainty in annual P_{CL} trends using the large ensemble of historical and future CMIP5 simulations. Given that we account for more than one realization per GCM and simulation type assessed, we can quantify the contribution of both internal variability and climate sensitivity to the dispersion obtained for the ensemble of runs (Datasets and methods). **Figure 11a** shows the modelled mean trends in annual P_{CL}, using 1960 as starting time and different years from 1980 to 2099 as the end for trends calculation. The standard deviation between the trends of the ensemble as well as the estimated contribution of natural variability to the this spread is shown in **Figure 11a** (dark grey). The remaining fraction of the ensemble spread is considered to account for the different P_{CL} sensitivities to the anthropogenic climate forcing (light grey in **Figure 11a**).

As expected, the uncertainty in the modelled P_{CL} change is reduced as the period considered for trend calculations increases and the role of internal variability weakens (**Figure 11a**). Thereby, the uncertainties in the P_{CL} projected to the end of the 21st century respond, principally, to differences in the GCMs' climate system characterization (the 'model uncertainty' after Hawkins and Sutton, 2011). We note that this spread, related to the distinct model P_{CL} sensitivities to anthropogenic forcing, is quite small compared to the precipitation change uncertainty in other regions of the globe (e.g., Boisier et al., 2015). Indeed, under a common socioeconomic scenario –RCP 8.5 in this case–, the direction of P_{CL} change (drying) is systematic across the GCMs assessed. Notwithstanding the consistency on the modelled century-long P_{CL} projections, natural variability remains an important source of uncertainty for trends computed in shorter time periods, in particular between 1960 and the present, warning us about the potentially mixed nature of the actual P_{CL} trend. A similar caveat has been pointed out in other regions having large natural climate variability (e.g., Deser et al, 2012).

The observations-based P_{CL} drying trends between 1960 and a year later than ~1990 are of clear larger amplitude than that simulated in most GCMs (red line in **Figure 11a**). In line with the uncertainties shown by the CMIP5 ensemble for trends computed in relatively short time periods (less than ~50 years), the year-to-year variation of the observed P_{CL} trends exposes the sensitivity of this metric to

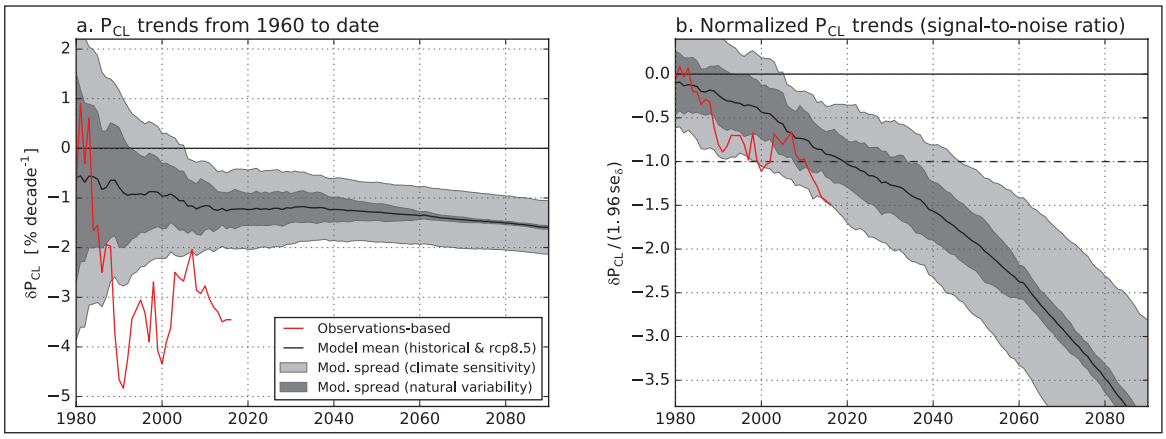

Figure 11: Uncertainties in observed and simulated changes in central-southern Chile precipitation. Multi-model mean (black) and observed (red) trends in central-southern Chile annual precipitation (δP_{CL}), computed between 1960 and the year indicated in the x-axis **(a)**. Shaded area indicates the simulated trend uncertainty (mean ± 1.0 standard deviation) derived from the ensemble of model simulations (Datasets and methods). Dark and light grey shading show de model spread fraction driven by natural variability and climate sensibility, respectively. Panel **(b)** shows the modeled (black) and observed (red) δP_{CL} normalized by 1.96 times the corresponding standard error of the trend (se_δ). A normalized δP_{CL} of magnitude larger than 1.0 corresponds to a trend statistically different from zero, with a confidence level of 95%. This threshold, indicated by the dashed line in panel (b), allows deducing the time of emergence (TOE) of changes in P_{CL}. DOI: https://doi.org/10.1525/elementa.328.f11

natural climate anomalies. In order to have a more robust metric of change, we normalized the value of a given trend by the trend error estimated for the corresponding regression slope ($\delta P_{CL}/1.96 se_\delta$; see Datasets and methods). These normalized trends represent signal-to-noise ratios, and show a more consistent pathway of change between models and the observations (**Figure 11b**). However, the observed normalized trend, of magnitude ~1.5 for 1960–2016, is still stronger than that derived for most CMIP5 models, even considering the range estimated for natural variability. In particular, this metric indicates that the long-term signal of P_{CL} change emerges from natural variability near the present time (a trend is considered to be significantly different from zero when the magnitude of the normalized trend exceeds the unity; this threshold is indicated by a dashed line in **Figure 11b**). The time of emergence (TOE) in models is centered in ~2020, while the observed P_{CL} indicates that the TOE has very likely been already reached.

This uncertainty assessment reinforces the conclusion that an anthropogenic change towards a dryer climate in central-southern Chile is underway. If the actual trends diagnosed with local rain-gauge records are correctly accounting for the strength of a regional-scale drying, then these results also suggest that the actual rainfall sensitivity in central-southern Chile to anthropogenic forcing is larger than those simulated in most CMIP5 models.

Concluding remarks

In this study, we presented an analysis based on a recently assembled rain-gauge and streamflow dataset within Chilean territory, showing a robust drying trend over the period 1960–2016 in a large region spanning 30°S to 48°S (the central and southern part of the country). Our results indicate that precipitation trends in this region have emerged above natural variability during the last decade. This signal is mainly driven by the rainfall decline observed in wet regions south of 37°S. The more episodic nature of precipitation in central Chile (30–37°S) makes any detection of change difficult. However, the negative rainfall trend in this region clearly agrees with the more robust change observed in river discharge data.

We also described a distinct seasonal signature on streamflow and precipitation trends, which unveil leading mechanisms of change and the role played by different large-scale climate forcings. In particular, the strong summer drying observed in southern Chile, of about 8% per decade, is coherent with well-known positive SAM-like changes in the southern hemisphere circulation. As reported earlier and as reassessed here with an ad-hoc set of climate simulations, the positive SAM-like circulation change in summer is, to a large degree, caused by stratospheric ozone depletion, amplifying the effect of the same sign that is driven by the GHG forcing in all seasons. Hence, in addition to precipitation change detection, we conclude that the main character of the observed long-term drying signal in Chile is attributable to anthropogenic forcing.

The SAM-congruent precipitation change is relevant for climate projections in Chile. Since the stratospheric ozone content is expected to recover throughout the 21st century as a result of the Montreal protocol, one can expect a lessening of the summer drying in southern Chile due to this forcing mechanism. The other important mode of variability that modulates precipitation variability at decadal scales in Chile is the PDO. The positive-to-negative phase transition of the PDO from the end of the 1970s to 2000s has largely contributed to the rainfall decline in central Chile in this period (Boisier et al., 2016), but not to the longer-term drying trend analyzed in this work. Yet, future changes in this mode of decadal variability will certainly modulate precipitation on top of the secular anthropogenic drying trend.

Besides the agreement on the sign and on the seasonal pattern of precipitation change shown by the observational and model data, the magnitude of the actual drying quantified in this study is substantially larger than that modelled. Our analysis indicates that this bias is unlikely to be fully explained by natural variability, implying that the current climate simulations may be underestimating the drying amplitude in central-southern Chile. Further research, looking deeper into the physical processes governing the Southeastern Pacific precipitation response to O_3, GHG and other climate forcings, is needed to constraint the uncertainties of the anthropogenic drying in Chile.

It is worth to recall that the changes in the precipitation regime are superimposed to a warming trend, so other aspects significant to regional hydro-climate and water availability should be considered, notably the increasing evapotranspiration and changes in annual cycle of snowmelt and runoff. Changes in temperature, in freezing level height and in rainfall extremes should also be accounted for when assessing risks of floods or droughts.

Regarding water availability in the coming decades, the take-home message for planning is that we can expect the anthropogenic drying trend to continue, although modulated on annual-to-decadal time scales by ENSO, the PDO and other sources of natural variability. The long-lasting and extended drought experienced in Chile in recent years serves as an analog for future climate. This phenomenon resulted in multiple often linked impacts affecting vegetation and watersheds (Garreaud et al, 2017), the biogeochemistry of coastal water (León-Muñoz et al., 2018; Aguirre et al., 2018), and the intensity of forest fires (Urrutia-Jalabert et al., 2018; González et al., 2018), stressing mutually-dependent effects of the drought on Chile's socio-ecosystems. Responses from the public and private sectors generally considered this drought to be a transient event. Moreover, current governance arrangements, i.e., more than 40 different national agencies with jurisdiction over water resources make coordinated action difficult and inefficient. As indicated by several authors (e.g., Van Loon et al, 2016; Aldunce et al., 2017; Crausbay et al., 2017), facing drought in the Anthropocene will require new, holistic approaches to water governance and climate change adaptation.

Data Accessibility Statement

Precipitation and streamflow data for Chile are available at: http://explorador.cr2.cl/. The CMIP5 data were acquired from the Earth System Grid Federation. https://esgf.llnl.gov.

Supplemental files

The supplemental files for this article can be found as follows:

- **Table S1.** List of climate models, simulations and ensemble members used in this study. DOI: https://doi.org/10.1525/elementa.328.s1
- **Figure S1.** Simulated precipitation trends. DOI: https://doi.org/10.1525/elementa.328.s1

Acknowledgements

We thank the Chilean agencies DGA and DMC, as well as the CR2 dataset and computing team, for maintaining, updating and providing rain-gauge and river streamflow data. We also acknowledge the World Climate Research Programme's Working Group on Coupled Modelling, which is responsible for CMIP, and we thank the climate modeling groups (listed in Table 1) for producing and making available their model output. For CMIP the U.S. Department of Energy's Program for Climate Model Diagnosis and Intercomparison provides coordinating support and led development of software infrastructure in partnership with the Global Organization for Earth System Science Portals. Comments and suggestions from two anonymous reviewers helped to improve an earlier version of this manuscript.

Funding information

This work has been developed within the framework of the CONICYT research center CR(2) (FONDAP 15110009) and the FONDECYT project 3150492 (JPB). RC and AD thank the support of CONICYT (Preis ACT1410, Preis 117 1690 and Preis 1151034) and the Universidad de Santiago de Chile (USACH, Preis USA1555).

Competing interests

The authors have no competing interests to declare.

Author contributions

- Contributed to conception and design: JPB, LG, RG, MR, RR
- Contributed to acquisition of data: JPB, CA, RC, AD
- Contributed to analysis and interpretation of data: JPB, CA, RC, AD, LG, RG, FL, CR, MR, RR
- Drafted and/or revised the article: JPB, CA, RC, AD, LG, RG, FL, CR, MR, RR
- Approved the submitted version for publication: JPB, CA, RC, AD, LG, RG, FL, CR, MR, RR

References

Aceituno, P. 1988. On the Functioning of the Southern Oscillation in the South American Sector. Part I: Surface Climate. *Mon Wea Rev* **116**(3): 505–524. DOI: https://doi.org/10.1175/1520-0493(1988)116<0505:OTFOTS>2.0.CO;2

Aceituno, P. 1998. Climate elements of the South American Altiplano. *Re. Geofis* **44**: 37–55.

Aceituno, P, Fuenzalida, H and **Rosenbluth, B.** 1993. Climate along the extratropical west coast of South America. In: *Earth system responses to global change: Contrasts between North and South America*, 61–72. In: Mooney, HA, Fuentes, ER and Kronberg, BI (eds.). Academic Press, NY.

Aguirre, C, García-Loyola, S, Testa, G, Silva, D and **Farias, L.** 2018. Insight into anthropogenic forcing on coastal upwelling off south-central Chile. *Elem Sci Anth* **6**(1): 59. DOI: https://doi.org/10.1525/elementa.314

Aldunce, P, Araya, D, Sapiain, R, Ramos, I, Lillo, G, Urquiza, A and **Garreaud, R.** 2017. Local Perception

of Drought Impacts in a Changing Climate: The Mega-Drought in Central Chile. *Sustainability* **9**(11): 1–15. DOI: https://doi.org/10.3390/su9112053

Allan, R and **Ansell, T.** 2006. A New Globally Complete Monthly Historical Gridded Mean Sea Level Pressure Dataset (HadSLP2): 1850–2004. *J Climate* **19**(22): 5816–5842. DOI: https://doi.org/10.1175/JCLI3937.1

Allen, MR and **Ingram, WJ.** 2002. Constraints on future changes in climate and the hydrologic cycle. *Nature* **419**(6903): 224–232. DOI: https://doi.org/10.1038/nature01092

Alvarez-Garreton, C, Mendoza, PA, Boisier, JP, Addor, N, Galleguillos, M, Zambrano-Bigiarini, M, Lara, A, Puelma, C, Cortes, G, Garreaud, R, McPhee, J and **Ayala, A.** 2018. The CAMELS-CL dataset: Catchment attributes and meteorology for large sample studies – Chile dataset. *Hydrol Earth Syst Sci Discuss* 1–40. DOI: https://doi.org/10.5194/hess-2018-23

Arblaster, JM and **Meehl, GA.** 2006. Contributions of External Forcings to Southern Annular Mode Trends. *J Climate* **19**(12): 2896–2905. DOI: https://doi.org/10.1175/JCLI3774.1

Barnes, EA, Barnes, NW and **Polvani, LM.** 2014. Delayed Southern Hemisphere Climate Change Induced by Stratospheric Ozone Recovery, as Projected by the CMIP5 Models. *J Climate* **27**(2): 852–867. DOI: https://doi.org/10.1175/JCLI-D-13-00246.1

Boisier, JP, Ciais, P, Ducharne, A and **Guimberteau, M.** 2015. Projected strengthening of Amazonian dry season by constrained climate model simulations. *Nature Clim Change* **5**(7): 656–660. DOI: https://doi.org/10.1038/nclimate2658

Boisier, JP, Rondanelli, R, Garreaud, RD and **Muñoz, F.** 2016. Anthropogenic and natural contributions to the Southeast Pacific precipitation decline and recent megadrought in central Chile. *Geophysical Research Letters* **43**(1): 413–421. DOI: https://doi.org/10.1002/2015GL067265

Bozkurt, D, Rojas, M, Boisier, JP and **Valdivieso, J.** 2018. Projected hydroclimate changes over Andean basins in central Chile from downscaled CMIP5 models under the low and high emission scenarios. *Climatic Change* **150**(3): 131–147. DOI: https://doi.org/10.1007/s10584-018-2246-7

Cai, W, Borlace, S, Lengaigne, M, Rensch, PV, Collins, M, Vecchi, G, Timmermann, A, Santoso, A, McPhaden, MJ, Wu, L, England, MH, Wang, G, Guilyardi, E and **Jin, F.** 2014. Increasing frequency of extreme El Niño events due to greenhouse warming. *Nature Climate Change* **4**(2): 111–116. DOI: https://doi.org/10.1038/nclimate2100

Cai, W, Cowan, T and **Thatcher, M.** 2012. Rainfall reductions over Southern Hemisphere semi-arid regions: The role of subtropical dry zone expansion. *Scientific Reports* **2**. DOI: https://doi.org/10.1038/srep00702

Cai, W, Whetton, PH and **Karoly, DJ.** 2003. The Response of the Antarctic Oscillation to Increasing and Stabilized Atmospheric CO_2. *J Climate* **16**(10): 1525–1538. DOI: https://doi.org/10.1175/1520-0442-16.10.1525

Christensen, JH, Krishna Kumar, K, Aldrian, E, An, S-I, Cavalcanti, IFA, de Castro, M, Dong, W, Goswami, P, Hall, A, Kanyanga, JK, Kitoh, A, Kossin, J, Lau, N-C, Renwick, J, Stephenson, DB, Xie, S-P and **Zhou, T.** 2013. Climate Phenomena and their Relevance for Future Regional Climate Change. In: *Climate Change 2013: The Physical Science Basis. Contribution of Working Group I to the Fifth Assessment Report of the Intergovernmental Panel on Climate Change*, Stocker, TF, Qin, D, Plattner, GK, Tignor, M, Allen, SK, Boschung, J, Nauels, A, Xia, Y, Bex, V and Midgley, PM (eds.). Cambridge University Press, Cambridge, United Kingdom and New York, NY, USA.

Cionni, I, Eyring, V, Lamarque, JF, Randel, WJ, Stevenson, DS, Wu, F, Bodeker, GE, Shepherd, TG, Shindell, DT and **Waugh, DW.** 2011. Ozone database in support of CMIP5 simulations: Results and corresponding radiative forcing. *Atmospheric Chemistry and Physics* **11**(21): 11267–11292. DOI: https://doi.org/10.5194/acp-11-11267-2011

Collins, M, Knutti, R, Arblaster, J, Dufresne, JL, Fichefet, F, Friedlingstein, P, Gao, X, Gutowski, WJ, Johns, T, Krinner, G, Shongwe, M, Tebaldi, C, Weaver, AJ and **Wehner, M.** 2013. Long-term climate change: Projections, commitments and irreversibility. In: *Climate Change 2013: The Physical Science Basis. Contribution of Working Group I to the Fifth Assessment Report of the Intergovernmental Panel on Climate Change*, Stocker, TF, Qin, D, Plattner, GK, Tignor, M, Allen, SK, Boschung, J, Nauels, A, Xia, Y, Bex, V and Midgley, PM (eds.), 1029–1136. Cambridge Univ. Press, Cambridge, U. K., and New York.

Compo, GP, Whitaker, JS, Sardeshmukh, PD, Matsui, N, Allan, RJ, Yin, X, Gleason, BE, Vose, RS, Rutledge, G, Bessemoulin, P, Brönnimann, S, Brunet, M, Crouthamel, RI, Grant, AN, Groisman, PY, Jones, PD, Kruk, M, Kruger, AC, Marshall, GJ, Maugeri, M, Mok, HY, Nordli, Ø, Ross, TF, Trigo, RM, Wang, XL, Woodruff, SD and **Worley, SJ.** 2011. The Twentieth Century Reanalysis Project. *QJR Meteorol Soc* **137**(654): 1–28. DOI: https://doi.org/10.1002/qj.776

CR2. 2015. Report to the Nation. The 2010-2015 megadrought: A lesson for the future. *Center for Climate and Resilience Research (CR2)* **28**. Available at: http://www.cr2.cl/wp-content/uploads/2015/11/InformeMegasequia_ingles_2016.pdf.

Crausbay, SD, Ramirez, AR, Carter, SL, Cross, MS, Hall, KR, Bathke, DJ, Betancourt, JL, Colt, S, Cravens, AE, Dalton, MS, Dunham, JB, Hay, LE, Hayes, MJ, McEvoy, J, McNutt, CA, Moritz, MA, Nislow, KH, Raheem, N and **Sanford, T.** 2017. Defining Ecological Drought for the Twenty-First Century. *Bull Amer Meteor Soc* **98**(12): 2543–2550. DOI: https://doi.org/10.1175/BAMS-D-16-0292.1

Demaria, EMC, Maurer, EP, Thrasher, B, Vicuña, S and **Meza, FJ.** 2013. Climate change impacts

on an alpine watershed in Chile: Do new model projections change the story? *Journal of Hydrology* **502**: 128–138. DOI: https://doi.org/10.1016/j.jhydrol.2013.08.027

Deser, C, Knutti, R, Solomon, S and **Phillips, AS.** 2012. Communication of the role of natural variability in future North American climate. *Nature Clim Change* **2**(11): 775–779. DOI: https://doi.org/10.1038/nclimate1562

Donat, MG, Lowry, AL, Alexander, LV, O'Gorman, PA and **Maher, N.** 2016. More extreme precipitation in the world's dry and wet regions. *Nature Clim Change* **6**(5): 508–513. DOI: https://doi.org/10.1038/nclimate2941

Eyring, V, Arblaster, JM, Cionni, I, Sedláček, J, Perlwitz, J, Young, PJ, Bekki, S, Bergmann, D, Cameron-Smith, P, Collins, WJ, Faluvegi, G, Gottschaldt, KD, Horowitz, LH, Kinnison, DE, Lamarque, JF, Marsh, DR, Saint-Martin, D, Shindell, DT, Sudo, K, Szopa, S and **Watanabe, S.** 2013. Long-term ozone changes and associated climate impacts in CMIP5 simulations. *Journal of Geophysical Research: Atmospheres* **118**(10): 5029–5060. DOI: https://doi.org/10.1002/jgrd.50316

Falvey, M and **Garreaud, R.** 2007. Wintertime Precipitation Episodes in Central Chile: Associated Meteorological Conditions and Orographic Influences. *Journal of Hydrometeorology* **8**(2): 171–193. DOI: https://doi.org/10.1175/JHM562.1

Fogt, RL, Perlwitz, J, Monaghan, AJ, Bromwich, DH, Jones, JM and **Marshall, GJ.** 2009. Historical SAM Variability. Part II: Twentieth-Century Variability and Trends from Reconstructions, Observations, and the IPCC AR4 Models. *J Climate* **22**(20): 5346–5365. DOI: https://doi.org/10.1175/2009JCLI2786.1

Garreaud, R, Lopez, P, Minvielle, M and **Rojas, M.** 2013. Large-Scale Control on the Patagonian Climate. *J Climate* **26**(1): 215–230. DOI: https://doi.org/10.1175/JCLI-D-12-00001.1

Garreaud, R, Vuille, M and **Clement, AC.** 2003. The climate of the Altiplano: Observed current conditions and mechanisms of past changes. *Palaeogeography, Palaeoclimatology, Palaeoecology* **194**(1): 5–22. DOI: https://doi.org/10.1016/S0031-0182(03)00269-4

Garreaud, RD, Alvarez-Garreton, C, Barichivich, J, Boisier, JP, Christie, D, Galleguillos, M, LeQuesne, C, McPhee, J and **Zambrano-Bigiarini, M.** 2017. The 2010–2015 megadrought in central Chile: Impacts on regional hydroclimate and vegetation. *Hydrol Earth Syst Sci* **21**(12): 6307–6327. DOI: https://doi.org/10.5194/hess-21-6307-2017

Garreaud, RD, Vuille, M, Compagnucci, R and **Marengo, J.** 2009. Present-day South American climate. *Palaeogeography, Palaeoclimatology, Palaeoecology* **281**(3): 180–195. DOI: https://doi.org/10.1016/j.palaeo.2007.10.032

Gillett, NP, Fyfe, JC and **Parker, DE.** 2013. Attribution of observed sea level pressure trends to greenhouse gas, aerosol, and ozone changes. *Geophys Res Lett* **40**(10): 2302–2306. DOI: https://doi.org/10.1002/grl.50500

Gillett, NP, Kell, TD and **Jones, PD.** 2006. Regional climate impacts of the Southern Annular Mode. *Geophysical Research Letters* **33**(23). DOI: https://doi.org/10.1029/2006GL027721

González, ME, Gómez-González, S, Lara, A, Garreaud, R and **Díaz-Hormazábal, I.** 2018. The 2010–2015 Megadrought and its influence on the fire regime in central and south-central Chile. Accepted for publication in *Ecosphere*.

Hagemann, S, Chen, C, Clark, DB, Folwell, S, Gosling, SN, Haddeland, I, Hanasaki, N, Heinke, J, Ludwig, F, Voss, F and **Wiltshire, AJ.** 2013. Climate change impact on available water resources obtained using multiple global climate and hydrology models. *Earth Syst Dynam* **4**(1): 129–144. DOI: https://doi.org/10.5194/esd-4-129-2013

Haylock, MR, Peterson, TC, Alves, LM, Ambrizzi, T, Anunciação, YMT, Baez, J, Barros, VR, Berlato, MA, Bidegain, M, Coronel, G, Corradi, V, Garcia, VJ, Grimm, AM, Karoly, D, Marengo, JA, Marino, MB, Moncunill, DF, Nechet, D, Quintana, J, Rebello, E, Rusticucci, M, Santos, JL, Trebejo, I and **Vincent, LA.** 2006. Trends in Total and Extreme South American Rainfall in 1960–2000 and Links with Sea Surface Temperature. *J Climate* **19**(8): 1490–1512. DOI: https://doi.org/10.1175/JCLI3695.1

Hawkins, E and **Sutton, R.** 2011. The potential to narrow uncertainty in projections of regional precipitation change. *Climate Dynamics* **37**(1): 407–418. DOI: https://doi.org/10.1007/s00382-010-0810-6

He, J and **Soden, BJ.** 2017. A re-examination of the projected subtropical precipitation decline. *Nature Climate Change* **7**(1): 53–57. DOI: https://doi.org/10.1038/nclimate3157

Held, IM and **Soden, BJ.** 2000. Water Vapor Feedback and Global Warming. *Annual Review of Energy and the Environment* **25**(1): 441–475. DOI: https://doi.org/10.1146/annurev.energy.25.1.441

Held, IM and **Soden, BJ.** 2006. Robust Responses of the Hydrological Cycle to Global Warming. *Journal of Climate* **19**(21): 5686–5699. DOI: https://doi.org/10.1175/JCLI3990.1

Ho, M, Kiem, AS and **Verdon-Kidd, DC.** 2012. The Southern Annular Mode: A comparison of indices. *Hydrol Earth Syst Sci* **16**(3): 967–982. DOI: https://doi.org/10.5194/hess-16-967-2012

IPCC. 2012. Managing the Risks of Extreme Events and Disasters to Advance Climate Change Adaptation. *A Special Report of Working Groups I and II of the Intergovernmental Panel on Climate Change*, Field, CB, Barros, V, Stocker, TF, Qin, D, Dokken, DJ, Ebi, KL, Mastrandrea, MD, Mach, KJ, Plattner, G-K, Allen, SK, Tignor, M and Midgley, PM (eds.), 582. Cambridge University Press, Cambridge, UK, and New York, NY, USA.

Jiménez Cisneros, BE, Oki, T, Arnell, NW, Benito, G, Cogley, JG, Döll, P, Jiang, T and **Mwakalila, SS.** 2014. Freshwater resources. In: Field, CB, Barros, VR, Dokken, DJ, Mach, KJ, Mastrandrea, MD, Bilir, TE, Chatterjee, M, Ebi, KL, Estrada, YO, Genova,

RC, Girma, B, Kissel, ES, Levy, AN, MacCracken, S, Mastrandrea, PR and White, LL (eds.), *Climate Change 2014: Impacts, Adaptation, and Vulnerability. Part A: Global and Sectoral Aspects. Contribution of Working Group II to the Fifth Assessment Report of the Intergovernmental Panel of Climate Change*, 229–269. Cambridge University Press: Cambridge, UK and New York, NY, USA.

Karpechko, AY, Gillett, NP, Marshall, GJ and **Scaife, AA.** 2008. Stratospheric influence on circulation changes in the Southern Hemisphere troposphere in coupled climate models. *Geophysical Research Letters* **35**(20). DOI: https://doi.org/10.1029/2008GL035354

León-Muñoz, J, Urbina, MA, Garreaud, R and **Iriarte, JL.** 2018. Hydroclimatic conditions trigger record harmful algal bloom in western Patagonia (summer 2016). *Scientific Reports* **8**(1): 1330. DOI: https://doi.org/10.1038/s41598-018-19461-4

Magrin, GO, Marengo, JA, Boulanger, J-P, Buckeridge, MS, Castellanos, E, Poveda, G, Scarano, FR and Vicuña, S. 2014. Central and South America. p. 1499–1566. In: Barros, VR, Field, CB, Dokken, DJ, Mach, KJ, Mastrandrea, MD, Bilir, TE, Chatterjee, M, Ebi, KL, Estrada, YO, Genova, RC, Girma, B, Kissel, ES, Levy, AN, MacCracken, S, Mastrandrea, PR and White, LL (eds.), *Climate Change 2014: Impacts, adaptation, and vulnerability. Part B: Regional Aspects. Contribution of Working Group II to the Fifth Assessment Report of the Intergovernmental Panel on Climate Change*. Cambridge University Press, Cambridge, UK.

Mantua, NJ, Hare, SR, Zhang, Y, Wallace, JM and **Francis, RC.** 1997. A Pacific Interdecadal Climate Oscillation with Impacts on Salmon Production. *Bull Amer Meteor Soc* **78**(6): 1069–1079. DOI: https://doi.org/10.1175/1520-0477(1997)078<1069:APICOW>2.0.CO;2

Marshall, GJ. 2003. Trends in the Southern Annular Mode from Observations and Reanalyses. *J Climate* **16**(24): 4134–4143. DOI: https://doi.org/10.1175/1520-0442(2003)016<4134:TITSAM>2.0.CO;2

Mekonnen, MM and **Hoekstra, AY.** 2016. Four billion people facing severe water scarcity. *Science Advances* **2**(2): e1500323. DOI: https://doi.org/10.1126/sciadv.1500323

Milly, PCD, Dunne, KA and **Vecchia, AV.** 2005. Global pattern of trends in streamflow and water availability in a changing climate. *Nature* **438**(7066): 347–350. DOI: https://doi.org/10.1038/nature04312

Minetti, JL, Vargas, WM, Poblete, AG, Acuña, LR and **Grande, GC.** 2003. Non-linear trends and low frequency oscillations in annual precipitation over Argentina and Chile, 1931–1999. *ATM* **16**(2). Available at: http://www.revistas.unam.mx/index.php/atm/article/view/8508.

MMA. 2016. Ministerio del Medio Ambiente. T*ercera Comunicación Nacional de Chile ante la Convención Marco de las Naciones Unidas sobre Cambio Climático*. Available at: https://unfccc.int/files/national_reports/non-annex_i_natcom/application/pdf/nc3_chile_19_december_2016.pdf.

Montecinos, A and **Aceituno, P.** 2003. Seasonality of the ENSO-Related Rainfall Variability in Central Chile and Associated Circulation Anomalies. *J Climate* **16**(2): 281–296. DOI: https://doi.org/10.1175/1520-0442(2003)016<0281:SOTERR>2.0.CO;2

Muñoz, AA, González-Reyes, A, Lara, A, Sauchyn, D, Christie, D, Puchi, P, Urrutia-Jalabert, R, Toledo-Guerrero, I, Aguilera-Betti, I, Mundo, I, Sheppard, PR, Stahle, D, Villalba, R, Szejner, P, LeQuesne, C and **Vanstone, J.** 2016. Streamflow variability in the Chilean Temperate-Mediterranean climate transition (35°S–42°S) during the last 400 years inferred from tree-ring records. *Climate Dynamics* 1–16. DOI: https://doi.org/10.1007/s00382-016-3068-9

OECD/ECLAC. 2016. OECD Environmental Performance Reviews: Chile 2016. Paris. Available at: http://www.oecd-ilibrary.org/environment/oecd-environmental-performance-reviews-chile-2016_9789264252615-en.

Polade, SD, Gershunov, A, Cayan, DR, Dettinger, MD and **Pierce, DW.** 2017. Precipitation in a warming world: Assessing projected hydro-climate changes in California and other Mediterranean climate regions. *Scientific Reports* **7**(1): 10783. DOI: https://doi.org/10.1038/s41598-017-11285-y

Poli, P, Hersbach, H, Tan, D, Dee, D, Thépaut, JN, Simmons, A, Peubey, C, Laloyaux, P, Komori, T, Berrisford, P, Dragani, R, Trémolet, Y, Hólm, E, Bonavita, M, Isaksen, L and **Fisher, M.** 2013. The data assimilation system and initial performance evaluation of the ECMWF pilot reanalysis of the 20th-century assimilating surface observations only (ERA-20C). *ERA Rep. Ser. 14*. ECMWF, Shinfield Park, Reading, U. K. Available at: http://www.ecmwf.int/en/research/publications.

Polvani, LM, Waugh, DW, Correa, GJP and **Son, S-W.** 2011. Stratospheric Ozone Depletion: The Main Driver of Twentieth-Century Atmospheric Circulation Changes in the Southern Hemisphere. *J Climate* **24**(3): 795–812. DOI: https://doi.org/10.1175/2010JCLI3772.1

Purich, A, Cowan, T, Min, S-K and **Cai, W.** 2013. Autumn Precipitation Trends over Southern Hemisphere Midlatitudes as Simulated by CMIP5 Models. *J Climate* **26**(21): 8341–8356. DOI: https://doi.org/10.1175/JCLI-D-13-00007.1

Quintana, JM and **Aceituno, P.** 2012. Changes in the rainfall regime along the extratropical west coast of South America (Chile): 30–43ºS. *Atmósfera* **25**(1): 1–22.

Rockström, J, Falkenmark, M, Allan, T, Folke, C, Gordon, L, Jägerskog, A, Kummu, M, Lannerstad, M, Meybeck, M, Molden, D, Postel, S, Savenije, HHG, Svedin, U, Turton, A and **Varis, O.** 2014. The unfolding water drama in the Anthropocene: Towards a resilience-based perspective on water for global sustainability. *Ecohydrology* **7**(5): 1249–1261. DOI: https://doi.org/10.1002/eco.1562

Rutllant, J and **Fuenzalida, H.** 1991. Synoptic aspects of the central chile rainfall variability associated with the southern oscillation. *Int J Climatol* **11**(1): 63–76. DOI: https://doi.org/10.1002/joc.3370110105

Schewe, J, Heinke, J, Gerten, D, Haddeland, I, Arnell, NW, Clark, DB, Dankers, R, Eisner, S, Fekete, BM, Colón-González, FJ, Gosling, SN, Kim, H, Liu, X, Masaki, Y, Portmann, FT, Satoh, Y, Stacke, T, Tang, Q, Wada, Y, Wisser, D, Albrecht, T, Frieler, K, Piontek, F, Warszawski, L and **Kabat, P.** 2014. Multimodel assessment of water scarcity under climate change. *PNAS* **111**(9): 3245–3250. DOI: https://doi.org/10.1073/pnas.1222460110

Shindell, DT and **Schmidt, GA.** 2004. Southern Hemisphere climate response to ozone changes and greenhouse gas increases. *Geophysical Research Letters* **31**(18). DOI: https://doi.org/10.1029/2004GL020724

Silvestri, GE and **Vera, CS.** 2003. Antarctic Oscillation signal on precipitation anomalies over southeastern South America. *Geophysical Research Letters* **30**(21). DOI: https://doi.org/10.1029/2003GL018277

Solomon, S, Ivy, DJ, Kinnison, D, Mills, MJ, Neely, RR and **Schmidt, A.** 2016. Emergence of healing in the Antarctic ozone layer. *Science*. DOI: https://doi.org/10.1126/science.aae0061

Son, S-W, Gerber, EP, Perlwitz, J, Polvani, LM, Gillett, NP, Seo, K-H, Eyring, V, Shepherd, TG, Waugh, D, Akiyoshi, H, Austin, J, Baumgaertner, A, Bekki, S, Braesicke, P, Brühl, C, Butchart, N, Chipperfield, MP, Cugnet, D, Dameris, M, Dhomse, S, Frith, S, Garny, H, Garcia, R, Hardiman, SC, Jöckel, P, Lamarque, JF, Mancini, E, Marchand, M, Michou, M, Nakamura, T, Morgenstern, O, Pitari, G, Plummer, DA, Pyle, J, Rozanov, E, Scinocca, JF, Shibata, K, Smale, D, Teyssèdre, H, Tian, W and **Yamashita, Y.** 2010. Impact of stratospheric ozone on Southern Hemisphere circulation change: A multimodel assessment. *Journal of Geophysical Research: Atmospheres* **115**(D3). DOI: https://doi.org/10.1029/2010JD014271

Taylor, KE, Stouffer, RJ and **Meehl, GA.** 2012. An Overview of CMIP5 and the Experiment Design. *Bull Amer Meteor Soc* **93**(4): 485–498. DOI: https://doi.org/10.1175/BAMS-D-11-00094.1

Trenberth, KE, Fasullo, J and **Smith, L.** 2005. Trends and variability in column-integrated atmospheric water vapor. *Climate Dynamics* **24**(7–8): 741–758. DOI: https://doi.org/10.1007/s00382-005-0017-4

Urrutia-Jalabert, R, González, ME, González-Reyes, Á, Lara, A and **Garreaud, R.** 2018. Climate variability and forest fires in central and south-central Chile. *Ecosphere* **9**(4): e02171. DOI: https://doi.org/10.1002/ecs2.2171

Van Loon, AF, Gleeson, T, Clark, J, Dijk, AIJMV, Stahl, K, Hannaford, J, Baldassarre, GD, Teuling, AJ, Tallaksen, LM, Uijlenhoet, R, Hannah, DM, Sheffield, J, Svoboda, M, Verbeiren, B, Wagener, T, Rangecroft, S, Wanders, N and **Van Lanen, HAJ.** 2016. Drought in the Anthropocene. *Nature Geoscience*. DOI: https://doi.org/10.1038/ngeo2646

Vera, CS and **Díaz, L.** 2015. Anthropogenic influence on summer precipitation trends over South America in CMIP5 models. *International Journal of Climatology* **35**(10): 3172–3177. DOI: https://doi.org/10.1002/joc.4153

Viale, M and **Garreaud, RD.** 2015. Orographic effects of the subtropical and extratropical Andes on upwind precipitating clouds. *Journal of Geophysical Research: Atmospheres* **120**(10): 4962–4974. DOI: https://doi.org/10.1002/2014JD023014

Vicuña, S, Garreaud, RD and **McPhee, J.** 2010. Climate change impacts on the hydrology of a snowmelt driven basin in semiarid Chile. *Climatic Change* **105**(3–4): 469–488. DOI: https://doi.org/10.1007/s10584-010-9888-4

Vicuña, S, McPhee, J and **Garreaud, RD.** 2012. Agriculture Vulnerability to Climate Change in a Snowmelt-Driven Basin in Semiarid Chile. *Journal of Water Resources Planning and Management* **138**(5): 431–441. DOI: https://doi.org/10.1061/(ASCE)WR.1943-5452.0000202

How to cite this article: Boisier, JP, Alvarez-Garreton, C, Cordero, RR, Damiani, A, Gallardo, L, Garreaud, RD, Lambert, F, Ramallo, C, Rojas, M and Rondanelli, R. 2018. Anthropogenic drying in central-southern Chile evidenced by long-term observations and climate model simulations. *Elem Sci Anth,* 6: 74. DOI: https://doi.org/10.1525/elementa.328

Domain Editor-in-Chief: Oliver Chadwick, Ph.D., Geography Department, University of California, Santa Barbara, US

Knowledge Domain: Earth and Environmental Science; Atmospheric Science

Part of an *Elementa* Special Feature: Regional manifestations of the Anthropocene: The case of Chile

Submitted: 01 June 2018 **Accepted:** 01 October 2018 **Published:** 07 December 2018

ELEMENTA Science of the Anthropocene

Elem Sci Anth is a peer-reviewed open access journal published by University of California Press.

OPEN ACCESS